Measures of Sympathetic and Parasympathetic Autonomic Outflow from Heartbeat Dynamics

Gaetano Valenza*, Luca Citi, J. Philip Saul, and Riccardo Barbieri

Abstract

Rationale: Reliable and effective non-invasive measures of sympathetic and parasympathetic peripheral outflow are of crucial importance in cardiovascular physiology. Although many techniques have been proposed to take up this long-lasting challenge, none has proposed a satisfying discrimination of the dynamics of the two separate branches. Spectral analysis of heart rate variability is the most currently used technique for such assessment. Despite its widespread use, it has been demonstrated that the subdivision in the low frequency (LF) and high frequency (HF) bands does not fully reflect separate influences of the sympathetic and parasympathetic branches, respectively, mainly due to their simultaneous action in the LF.

Objective: Two novel heartbeat-derived autonomic measures, the Sympathetic Activity Index (SAI) and Parasympathetic Activity Index (PAI), are proposed to separately assess the time-varying autonomic nervous system (ANS) synergic functions. Their efficacy is validated in landmark autonomic manoeuvres generally employed in clinical settings.

Methods and Results: The novel measures move beyond the classical frequency domain paradigm through identification of a set of coefficients associated with a proper combination of *Laguerre* base functions. The resulting measures were compared to the traditional LF and HF power. A total of 236 ECG recordings were analyzed for validation, including autonomic outflow changes elicited by procedures of different nature and temporal variation, such as postural changes, lower body negative pressure, and handgrip tests.

Conclusions: The proposed SAI-PAI measures consistently outperform traditional frequency-domain indices in tracking expected instantaneous autonomic variations, both vagal and sympathetic, and may aid clinical decision making showing reduced inter-subject variability and physiologically-plausible dynamics.

Index Terms

Heart Rate Variability (HRV), Autonomic Nervous System, Sympatho-Vagal Balance, Laguerre expansion, Sympathetic Activity Index (SAI), Parasympathetic Activity Index (PAI).

I. New & Noteworthy

While it is possible to obtain reliable estimates of parasympathetic activity from the ECG, a satisfying method to disentangle the sympathetic component from HRV has not been proposed yet. To overcome this long-lasting limitation, we propose two novel HRV-based indices, the Sympathetic and Parasympathetic Activity Index.

* Corresponding author: Gaetano Valenza, Ph.D.
Bioengineering and Robotics Research Center E. Piaggio
and Department of Information Engineering,
University of Pisa, Largo Lucio Lazzarino 1,
56122, Pisa, Italy.
Email: g.valenza@ieee.org

Gaetano Valenza is with the Computational Physiology and Biomedical Instruments group at the Bioengineering and Robotics Research Center E. Piaggio and Department of Information Engineering, University of Pisa, Largo Lucio Lazzarino 1, 56122, Pisa, Italy. Email: g.valenza@ieee.org

L. Citi is with the School of Computer Science and Electronic Engineering, University of Essex, Colchester, UK.

J.P. Saul is with West Virginia University School of Medicine, USA.

R. Barbieri is with the Department of Electronics, Informatics and Bioengineering, Politecnico di Milano, Milano, Italy.

G. Valenza and R. Barbieri are with the Department of Anesthesia, Critical Care and Pain Medicine, Massachusetts General Hospital, Boston, MA, USA.

II. Introduction

Heartbeat dynamics and its spontaneous fluctuations are directly controlled by autonomic nervous system (ANS) outflow to the heart [26]. Specifically, the multi-path feedback system for neural control of the heart is manifested by the complex interaction between the sympathetic and parasympathetic (vagal) limbs of the ANS [43]. Typically, for cardiovascular control, the sympathetic system is activated during the so-called "fight-or-flight" reactions, when there are drops in arterial pressure due to gravitational changes and during exercise, whereas the parasympathetic system is predominates during a variety of resting conditions. The two systems generally act complementary, i.e. the increase of one usually corresponds to a decrease of the other; however, they present quite different temporal dynamics mainly due to the different response properties of the two systems.

Sympathetic and parasympathetic activity interact to modify sinus node activity and produce the time-varying spontaneous variability of heart rate (HR), which is modulated by three major physiological factors: blood-pressure control, thermal regulation, and respiration. Indeed, the cardiovascular homeostatic control is directed at maintaining arterial blood pressure according to peripheral blood flow demand.

Accordingly, in many cardiovascular diseases, abnormalities of autonomic cardiac control play an important role in the development and/or in the progression of the underlying pathological process. Examples include hypertension [18], [31], major depression [57], cirrhosis and ascites [16], obesity [15], [56], diabetes [13], [15], and heart failure [25], [35]. Because the two systems might be differently affected by pathological outcomes, significant cardiovascular research has been focused on the reliable and effective assessment of the separate influences of parasympathetic and sympathetic neural pathways [2], [3], [19], [27], [33], [36], [38], [40], [47].

In this study we present a novel parametric model of cardiovascular control, based on a specific combinatorial use of orthonormal Laguerre Functions. This unique representation is able to separately characterize sympathetic and parasympathetic activity by using only the timing of heartbeats. The rationale behind the proposed SAI-PAI approach starts from the observation that the cholinergic and adrenergic drives have different temporal dynamics, partly overlapping in the frequency domain. For this reason, instead of base functions defined in limited frequency ranges (like the sinusoids for a simple frequency transform), a proper weighted sum and/or subtraction of primitives unselectively spanning the frequency domain would be able to decompose the heartbeat variability due to ANS activity by disentangling the unique contribution of each autonomic branch. Such primitives can be defined from discrete-time orthonormal Laguerre bases, which for a given α have equal magnitude and different phase spectra in the frequency domain [32], [34], [53].

Technically, heartbeat series are convolved through the Laguerre Functions in order to identify personalized time-varying Laguerre coefficients which are embedded in an autoregressive model combining the input data. Finally, a specifically tailored combination of the Laguerre coefficients defines two independent measures: the Sympathetic Activity Index (SAI) and the Parasympathetic Activity Index (PAI). According to the estimation method chosen to derive the Laguerre coefficients, it is possible to obtain finite SAI and PAI estimates within a given observation in time, e.g. by using least square and maximum likelihood estimation methods, to obtain beat-to-beat SAI and PAI estimates in time, e.g. by using, Kalman filtering, or to obtain instantaneous SAI and PAI estimates in time by using point-process modeling [7], [53].

The presented results are aimed at comparing the new definitions of ANS activity with current frequency-based methods in several ECG studies involving sympatho-vagal modulations induced by postural changes (standing, slow tilting and fast tilting) [53], selective autonomic blockade [41], lower body negative pressure [61], [62], and handgrip [61], [62].

We show experimental results on SAI, PAI, as well as LF and HF powers using time-varying estimates gathered from Kalman and point-process methods. When possible, we emphasize the use of point-process statistics for the SAI and PAI estimates because of several advantages [7], [53]: i) from the event-related structure of the R-waves, this approach provides instantaneous heartbeat estimates in the time and frequency domains; ii) it assesses the model goodness-of-fit [7], [53], *i.e.* how well a given model describes the observed R-R interval series; and iii) there is no need for interpolation methods to be applied on the original RR interval series. Note that our point-process modeling is based on a physiological plausible, history-dependent inverse Gaussian probability functions [7], [14], [53].

The manuscript is organized as follows: Section III briefly describes the fundamental physiology of the sympathetic and parasympathetic nervous systems, Section IV reports on the current state of the art of estimation of ANS dynamics from heartbeats, Section V explains technical details on the SAI and PAI estimation based on Laguerre functions, Sections VI and VII describe data and results, respectively, related to the several experimental protocols employed for the measures validation, and Section VIII contains the discussion and conclusions.

III. Physiology of the Sympathetic and Parasympathetic Systems at a Glance

The sympathetic and parasympathetic nervous systems are quite different functionally, anatomically and physiologically. Both systems carry sensory (afferent) signals to the brain and spinal cord, and efferent signals from the brain to the target organs. The Central Nervous System (CNS) control comes mostly from the hypothalamus, with inputs also from the limbic system and the reticular activating system [46]. The nucleus of the solitary tract in the medulla is the primary site of termination

of cardiopulmonary afferents from cranial nerves involved in brainstem reflex control. Here, the connection between the CNS and its effector consists of two kinds of neurons: the pre-ganglionic neuron and the post-ganglionic neuron. The synapses between these two neurons lie outside the CNS, in autonomic ganglia.

The parasympathetic system originates in the brainstem (cranial nerves III, VII, IX, and X) and sacral region of the spinal cord ($S2 - S4$). The functions associated with this system are basically related to rest and digestive activity. Non-cardiopulmonary parasympathetic control is involved in salivation, production of digestive enzymes, peristalsis, urination and defecation. Cardiopulmonary actions include reducing HR and blood pressure, reducing the respiratory rate, and conserving energy through relaxation and rest. The principal neurotransmitter is acetylcholine, released from both the preganglionic and the postganglionic neurons, and binding to cholinergic receptors. For the organism as a whole, the most important part of this system is the vagus nerve, which supplies parasympathetic signals to almost all the organs of the thorax and abdomen.

The sympathetic system originates in the thoracic and lumbar regions of the spinal cord ($T_1 - L_2$). The role of this system is related to the so called 'fight-or-flight' response. Thus, the sympathetic system prepares the body for situations requiring alertness or strength, or situations that arouse fear, anger, excitement, or embarrassment. In these kind of situations, the sympathetic nervous system may increase the HR, causes dilation of the bronchioles of the lungs (increasing oxygen intake), and contributes to dilation of blood vessels that supply the heart and skeletal muscles (increasing blood supply) while decreasing blood supply to organs not involved in the response (e.g., gut). The adrenal medulla is stimulated to release epinephrine (adrenaline) and norepinephrine (noradrenalin), which in turn increases the metabolic rate of cells and stimulates the liver to release glucose into the blood. Sweat glands are stimulated to produce sweat. The sympathetic nervous system afferents are also responsible for the transmission of visceral pain from organs such as the gut, bladder and uterus.

Many functions of the sympathetic nervous system oppose those of the parasympathetic nervous system. Although it is noteworthy that not all organs receive innervation from both components of the ANS, it is quite often the case that multiple interactions between the two systems result in a nonlinear transmission of neural information to the organ of interest. A good example of such interaction is evident in considering the autonomic outflow to the heart.

In fact, the sympathetic and parasympathetic branches, through their continuous dynamic interaction, modulate the HR response by means of the so-called bidirectional augmentation [45]: during a predominant sympathetic control, a concomitant tonic vagal signal increases the gain of the transfer function relating dynamic sympathetic stimulation to HR, and viceversa (during a predominant parasympathetic control, a concomitant tonic sympathetic signal increases the gain of the transfer function relating dynamic vagal stimulation to HR). Such a bidirectional augmentation is mediated by cytosolic adenosine 3',5'-cyclic monophosphate (cAMP), which constitutes a component of the biological basis of nonlinear autonomic control on heartbeat dynamics.

IV. Estimation Methods of Sympathetic and Parasympathetic Peripheral Outflow in Humans

Several methodologies for the assessment of sympathetic and parasympathetic activity in humans have been proposed throughout the past decades. Historically, measurement of plasma noradrenaline have represented a gold standard for the quantification of sympathetic neural functions [19]. More recently, direct recording of sympathetic nerve activity via microneurography, direct catecholamine measurements, and noradrenaline radiotracer have largely supplanted the plasma noradrenaline approach [19]. Neural imaging techniques also allow for direct visualization of sympathetic innervation of human organs, providing information on the *in vivo* metabolism of noradrenaline in different cardiovascular regions [19]. However, such techniques require expensive equipment and technical support, and are not useful for assessing daily activities as do devices such as a Holter monitor or other miniaturized wearable devices. Furthermore, power spectral density analysis of electrodermal activity has been recently proposed for the assessment of sympathetic functions [37].

A. Current Autonomic Estimates using Heart Rate Variability and the Frequency Domain Paradigm

Despite being widely introduced into the scientific practice and literature, the methods of autonomic activity evaluation noted above are not commonly used in clinical settings [19]. Conversely, processing of heart rate data, commonly measured by detecting R-waves from the electrocardiogram (ECG), and the superimposed instantaneous heartbeat variations, referred to as Heart Rate Variability (HRV) has been of growing importance in the attempt to develop real-time applications which use simple, non-invasive sensors in clinical and non-clinical settings [38], [44], [47]. In fact, monitors of cardiovascular variability based on standard clinical multichannel signal acquisition equipment, single-channel miniature devices, smartphones, or wearable technology for ambulatory monitoring, have been effectively used in numerous settings, including the intensive care unit, the operating room, during normal daily activities, sleep, exercise and during changes in emotional state, or well-being states (see [38], [40], [47] for reviews including many other applications).

From a technical point of view, the most widely used methodology to quantitatively assess ANS dynamics is based on a frequency-domain analysis, *i.e.* computing the HRV power spectral density [2], [3], [27], [36], [38], [47]. Specifically, power in the high frequencies (HF: 0.15-0.4 Hz) of the HRV comprises respiratory-associated oscillations, which are mediated via the vagus nerve. Of note, the modulation of HR due to respiratory drive to cardiac vagal motor neurons refers to the so-called respiratory sinus arrhythmia [3], [38], [47], [65]. Slower oscillations in the low frequencies (LF: 0.04-0.15 Hz) reflect to some

extent slower closed-loop compensatory changes of blood pressure and HR mediated through the baroreflex, and involving both autonomic branches (sympathetic and parasympathetic drive) [2], [3], [27], [36], [38], [47].

Specifically, the LF rhythm (centered at 0.1 Hz) of HRV is mainly due to arterial baroreflex modulation. It is also dramatically affected by the presence of vasomotor noise, which is amplified by the resonance in the baroreflex loop, placed around 0.1 Hz. Previous studies [1], [28], [30] suggested that the LF component of the power spectrum of HRV is strongly affected by the sympathetic system as changes in the sympathetic gains cause a significant alteration in this component of the spectrum. However, it is clear that changes below 0.15 Hz can be and are mediated by both cardiac vagal and sympathetic activity [41]. Furthermore, recent evidences and meta-analyses point out that how the HRV-LF band can be dramatically affected by parasympathetic dynamics [17], [39].

The HRV-HF components ($>$0.15 Hz) are determined by two concurrent mechanisms. The first is the effect of systemic arterial pressure changes mediated by the baroreflex. Such a pressure exhibits respiratory fluctuations caused by the intrathoracic and abdominal pressure changes (mechanical effect) and by the lung stretch receptor reflex working on resistance (neurogenic effect). These fluctuations systematically stimulate the baroreflex at the respiratory period. In this high frequency band, however, the baroreflex works entirely through its strong and fast vagal component, whereas the sympathetic component is almost completely suppressed because of its low-pass filtering dynamics. The second mechanism, is due to a combination of the lung stretch receptor reflex effect on vagal activity and respiratory related brain stem gating of vagal outflow. A common and widely accepted viewpoint in the literature is that the HF peak and power in the HRV-HF band can always be considered as a reliable index of vagal activity [17], [38], [39], [47], [50]. Nevertheless, the HF peak is modulated by all factors affecting the input to baroreflex and the lung stretch reflex (such as the depth and frequency of breathing [22], venous compliances in the thoracic and abdominal cavity, posture changes [48], *etc.*) and depends strongly on the sensitivity of the cardiac pacemaker to efferent activity. Hence, as suggested by Akselrod [1] and Malpas [30], in different subjects and/or under different breathing conditions, the HF spectral component may be largely different even in the presence of an equivalent vagal gain. Importantly, due to the mentioned ambiguity of the LF and HF power indices, Malliani *et al.* [29] proposed the ratio of the LF power to HF power (hereinafter LF/HF) as an index of sympatho-vagal balance. Note that the use of LF/HF ratio to assess the sympathetic and parasympathetic balance has also been challenged [17], [39].

Despite the mentioned references and its widespread use, HRV spectral analysis is far from being a definitive, reliable methodology for the non-invasive assessment of ANS functions. This has been known since more than twenty years. As a matter of fact, a review on how to assess sympathetic activity in humans from Grassi *et al.* in 1999 [19] reports: "[...] the approach based on spectral analysis of HR and blood pressure signals has been shown to have important limitations which prevent the method from faithfully reflecting sympathetic cardiovascular drive."

To date, standard HRV-based approaches have not been able to provide measures of autonomic activity which overcome the large variability between normal subjects, thus limiting their use in clinical settings. A few investigations have attempted to overcome this significant limitation. Specifically, Vetter *et al.* proposed to quantify the ANS activity using a blind source separation technique of HR and blood pressure variability [58], as well using HR and QT waves intervals variability [59], whereas, more recently, Chen *et al.* [10] derived ANS activity indices based on a multi-signal analysis of the R-R variability by processing the HR, blood pressure, and the instantaneous lung volume. Similarly, Xiao *et al.* [63], [64] represented sympathetic and parasympathetic functions modeling the coupling mechanism between lung volume and HR. Although these sophisticated methods might have been successful in separating sympathetic and parasympathetic dynamics, they do require recordings of multiple physiological parameters to obtain the estimations.

Concerning the use of RR interval series exclusively, Chon *et al.* introduced a principal dynamic mode analysis of HRV to separately characterize the sympathetic and the parasympathetic activity [66], [67]. However, the authors reported that the algorithm requires proper calibration and that a broadband HR spectrum is a strict requirement of such principal dynamic modes, a condition which may not be satisfied in some subjects [66].

To summarize, despite a few encouraging attempts, no methodology to date has been able to provide a separate, simultaneous, independent assessment of sympathetic and vagal instantaneous dynamics that can be (a) obtained exclusively from the heartbeat, (b) applied to a wide range of subjects, (c) specifically tailored to the individual, and (d) allowing for time-varying/instantaneous quantification (see [8] for review).

V. Derivation of the Novel Sympathetic and Parasympathetic Activity Measures

The 'classic' frequency-domain characterization is based on the Fourier transform, an operator which represents HRV in the frequency-space. The base functions of this space are defined by each sample along frequency. In the HRV case, these values are 'grouped' by frequency range (VLF, LF, HF) as recommended in a 1996 guidelines document [47]. The Autoregressive formulation has the property of reducing the dimensionality of the frequency-space by defining a limited number of preferred oscillations (associated with the poles of the transfer function) dependent on the autoregression order. The variability related to each pole is then univocally associated to a specific frequency, and can only be accounted for within each respective frequency range (again VLF, LF, HF). This model has been of great success in many applications for autonomic assessment, as the frequencies/poles within the HF frequency range have been directly associated with vagal dynamics in several instances. On

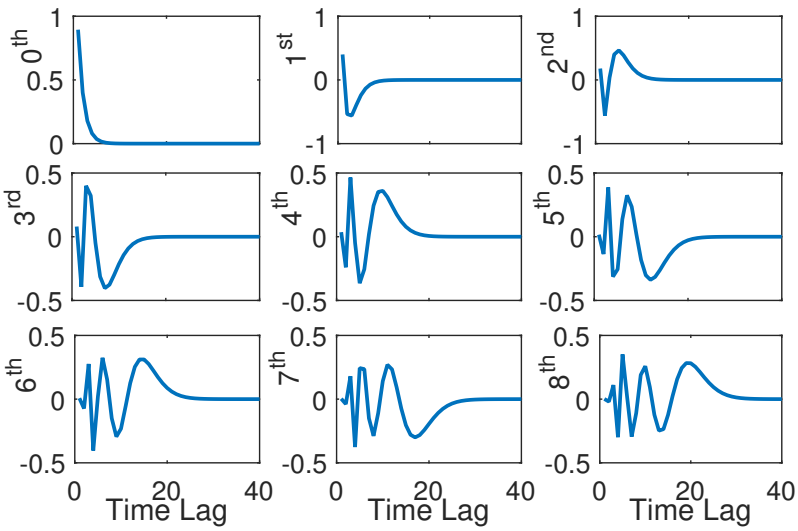

Fig. 1. Laguerre polynomials of order 8 for $\alpha = 0.2$ plotted over the first 40 lags.

the other hand, important limitations of such frequency subdivision have been recently pointed out [17], [19], [39], the most important being related to the fact that the LF range contains both vagal and sympathetic dynamics, and that respiratory dynamics shifts to the LF range would consequently affect the HF quantification of vagal influence. The primary rationale of this study is to overcome limitations imposed by the artificial separation of frequency ranges by defining a model whose base functions are not defined in the frequency domain, Laguerre functions, which are a set of mathematical functions of time. Laguerre functions are characterized by a specific “order" (which can vary from zero to any other positive integer number), and a specific value “α" which characterizes fine modulation of the number of oscillations across zero, as well as very specific time responses. If we multiply two Laguerre functions of any order, the area under the curve is zero, a function of the property of “orthogonality". These functions are adopted as the base functions of a “new" Laguerre-space.

The proposed SAI and PAI measures are derived characterizing and predicting each heartbeat event given a combination of past information expressed as cardiovascular variability. Such formulation has been shown to improve the model parameter identification and reduce the number of parameters to be estimated [32], [34], [53].

Since the RR intervals constitute the observation values used to estimate the model, the Laguerre-based characterization and prediction of heartbeat events by definition embed both sympathetic and parasympathetic information. Most importantly, the SAI collects a combination of Laguerre functions with slow responses (reflecting the slower conduction velocity associated with the sympathethic nerve), whereas the PAI combines contributions from Laguerre functions of higher order, thus representing responses along the entire frequency range (and not only HF as in the standard spectral identification). As described below, a pharmacological autonomic blockade protocol was used as the training set to identify isolated dynamics. In this stage, extensive analysis was performed in confirming the effectiveness of the Laguerre-derived dynamics to separate the two cardiovascular autonomic outflows, and consequently identify the best combinatorial coefficients.

A. Derivation Methodology

As noted in the Introduction, the scientific rationale behind the hereby proposed measures of autonomic activity, SAI and PAI, relies on a proper combination of the so-called Laguerre coefficients, derived from the use of Laguerre functions, which have unique properties in the time and frequency domains, as well as in their high-order statistics [32], [34], [53].

Block schemes of all the methodological stages involved in the SAI-PAI estimation are described in Figs 3 and 4 of the Supplementary Materials.

The j^{th}-order discrete-time orthonormal Laguerre function is defined as follows:

$$\phi_j(n) = \alpha^{\frac{n-j}{2}}(1-\alpha)^{\frac{1}{2}} \sum_{i=0}^{j} (-1)^i \binom{n}{i} \binom{j}{i} \alpha^{j-i}(1-\alpha)^i, (n \geq 0)$$

Figure 1 shows the first Laguerre Functions for a given α value ($0 < \alpha < 1$), which determines the rate of exponential asymptotic decline of these functions.

Given a set of K heartbeat events $\{u_k\}_{k=1}^{K}$ (*e.g.,* R-waves from the ECG), let $RR_k = u_k - u_{k-1} > 0$ denote the k^{th} RR interval, or equivalently, the waiting time until the next R-wave event.

Here, we propose to model heartbeat dynamics with $\mu_{RR}(t, \mathcal{H}_t, \xi(t))$ at each time t as function of past RR intervals along with the Laguerre expansion. We take one step further and try to separate the influence of the sympathetic and parasympathetic system to the $\mu_{RR}(t, \mathcal{H}_t, \xi(t))$ estimation. Hence:

$$\mu_{RR}(t, \mathcal{H}_t, \xi(t)) = g_0(t) + \underbrace{\sum_{j=0}^{P_{\text{Symp}}} g_1(j,t)\, l_j(t)}_{\textit{Sympathetic}} + \underbrace{\sum_{j=P_{\text{Symp}}+1}^{P_{\text{ParSymp}}} g_1(j,t)\, l_j(t)}_{\textit{Parasympathetic}} \tag{1}$$

where

$$l_j(t) = \sum_{n=1}^{\widetilde{N}(t)} \phi_j(n) RR_{\widetilde{N}(t)-n} \tag{2}$$

is the j^{th}-order Laguerre filter output, and $\widetilde{N}(t)$ denotes the index of the previous R-wave event occurred before time t, $\mathcal{H}_t = (u_k, RR_k, RR_{k-1}, ..., RR_{k-K+1})$ is the history of all previous RR intervals before time t, and $\xi(t) = \{g_0(t), g_1(t)\}$ is the vector of the time-varying Laguerre coefficients to be estimated.

In an attempt to match the frequency response of the Laguerre filters with the dynamic response of the sympathetic and the parasympathetic systems [2], [3], [27], [36], [38], [41], [47], we have chosen $P_{\text{Symp}} = 1$ and $P_{\text{ParSymp}} = 8$. After preliminary testing on synthetic and experimental data (not shown), $\alpha = 0.2$ was chosen for the SAI and PAI derivation.

Finally, the definition of the SAI and PAI as a combination of disentangled Laguerre coefficients $\{g_1\}$ is as follows:

$$SAI(t, \xi(t)) = \Psi_{S_0} + \sum_{j=1}^{N_1} \Psi_{S_j}\; g_1(j-1, t) \tag{3}$$

$$PAI(t, \xi(t)) = \Psi_{P_0} + \sum_{j=1}^{N_2} \Psi_{P_j}\; g_1(j + (P_{\text{Symp}} + 1), t) \tag{4}$$

with $N_1 = P_{\text{Symp}} + 1$ and $N_2 = P_{\text{ParSymp}} - (P_{\text{Symp}} + 1)$.

Thanks to its parametric structure, the model-defined parameters can be updated along time using the most efficient and popular methods reported in recent literature for recursive parameter estimation.

However, by using the point-process modeling, the Laguerre coefficients and, consequently, $\mu_{RR}(t, \mathcal{H}_t, \xi(t))$, $SAI(t, \xi(t))$, and $PAI(t, \xi(t))$ can be defined in a continuous-time fashion, thus obtaining instantaneous autonomic activity measures at a very fine timescale with no interpolation between the arrival times of two beats.

In this study, the estimation of all model coefficients, including Laguerre coefficients $\{g_1\}$, was performed using a local maximum-likelihood estimation method. Additionally, model goodness-of-fit was based on the Kolmogorov-Smirnov (KS) tests and associated KS statistics [7]. Particularly, the recursive, causal nature of the estimation allows for prediction of each new observation, given the previous history, independently at each iteration. The model and all its parameters are therefore also updated at each iteration without priors. Autocorrelation plots were also utilized to test the independence of the model-transformed intervals [7]. Exhaustive mathematical details on this matter are reported in the Supplementary Materials.

Optimal estimation of the Ψ_S and Ψ_P coefficients is a critical aspect in the proposed methodology. In fact, these values determine the capability of the algorithm to separate the sympathetic and parasympathetic components, both embedded in the disentangled Laguerre coefficients g_1. The Ψ_S and Ψ_P coefficients were obtained from respective sympathetic and parasympathetic blockades. Then, averaged values from subjects were fixed and used to obtain the linear impulse response functions from the Laguerre expansion approach.

In order to find unique Ψ_S and Ψ_P coefficients of broad applicability, *i.e.* suitable for a generic human subject, a specific a priori estimation was performed using a multiple linear regression technique on data involving selective autonomic blockade during postural changes (see [41] for experimental details). This dataset was used as a training set by following the procedure, which is summarized as follows:

- ECG data was utilized from 7 healthy subjects with atropine-induced parasympathetic blockade during a supine resting state and after a postural change by standing test.
- These data from each subject were used to derive the "purely" sympathetic coefficients $\{\Psi_S(j,n)\}_{n=1}^{N}$ by means of multiple linear regression considering a step function template having low value throughout the supine resting state, and high value throughout the standing phase after standing.
- Coefficients of general applicability for the sympathetic activity were then obtained through the average among subjects: $\{\Psi_{S_j}\} = \langle\{\Psi_S(j,n)\}_{n=1}^{N}\rangle_N$.

Likewise, the "purely" parasympathetic coefficients $\{\Psi_{P_j}\}$ were obtained by averaging among 7 subjects using data gathered during sympathetic blockade, which was induced through a bolus of propranolol, and performing a multiple linear regression of a step function template having high value throughout the supine resting state, and low value throughout the standing phase after standing. Estimated coefficients are reported in Section VII-A. Further test and validation datasets follow below.

VI. Experimental Setup

Autonomic activity measures were validated by analysing an extensive collection of experimental ECG data, and comparing SAI, PAI, and their ratio SAI/PAI with LF and HF power, and their ratio LF/HF derived from standard frequency domain analyses. Experimental recordings were gathered during maneuvers which are well known in the literature to induce strong sympatho-vagal changes. These 'gold-standard' studies for assessing autonomic activity are as follows: tilt-table protocols including i) stand-up, ii) slow tilt (*i.e.* 50 s from 0 to 70 degrees) and iii) fast tilt (*i.e.* 2 s from 0 to 70 degrees); iv) supine and standing during full autonomic blockade; v) lower body negative pressure test; vi) and handgrip test.

Details on these experimental protocols follow below.

A. Tilt-table protocol

A single-lead ECG was continuously recorded from 10 healthy subjects undergoing a tilt-table protocol. Each subject was first placed horizontally in a supine position, with restraints used to secure him/her at the waist, arms, and hands. The subject was then tilted from the horizontal to the vertical position and returned to the horizontal position either through a "slow" tilt (50 s from 0 to 70 degrees), or "fast" (*i.e.* 2 s from 0 to 70 degrees). Stand-up sessions were also included.

The study was conducted at the Massachusetts Institute of Technology (MIT) General Clinical Research Center (GCRC) and was approved by the MIT Institutional Review Board and the GCRC Scientific Advisory Committee. Subjects were five men and five women: age (mean$\pm$SD) 28.7$\pm$1.2 yr. Each subject performed six sessions (two stand-up, two slow tilt, and two fast tilt) remaining in each upright state for 3 min. The protocol lasted 55–75 min (3,300–4,500 s).

Resting state is known to be associated with a dominant vagal activity, whereas states after tilting are known to be associated with a dominant sympathetic activity.

Full details on this experimental protocol can be found in [7], [20], [21], [53].

B. Lower Body Negative Pressure (LBNP)

Fifty-eight healthy controls between 12 and 18 years volunteered from schools in Oslo, Norway. Controls having a chronic disease (such as allergy) or using drugs (including contraceptive pills) on a regular basis were excluded for the study. One week before the experiments, all participants were instructed not to drink beverages containing alcohol or caffeine, not to take any drugs, and not to use tobacco products. They were instructed to fast overnight the day before the experiments. Written, informed consent was obtained from all participants and their parents. The study complied with the Declaration of Helsinki and was approved by the regional committee for ethics in medical research. Experiments started at 11 a.m. The participants had been offered a light meal 2 hours before, but were not allowed to eat or drink otherwise. They lay supine with their lower body in a plastic chamber from which air could be evacuated very rapidly, reaching a predefined negative pressure within milliseconds. They were familiarized with the test situations in 2 pilot experiments. Five minutes were used for baseline recording (resting state). Then, LBNP of -20 mm Hg was applied for 6 minutes. All subjects but one performed this procedure twice with continuous ECG recordings. Eight additional recordings were excluded from the analyses due to low technical quality, therefore the total number of recordings used for this study was 106.

It is known that the resting state is associated with a dominant vagal activity, whereas the LBNP state is associated with a dominant sympathetic activity. Full details on this experimental protocol can be found in [61], [62].

C. Handgrip

The same subjects who performed the LBNP described in the previous paragraph also underwent a handgrip experimental procedure. Handgrip is a common test for studies of cardiovascular adjustments during isometric exercise. During handgrip, the cardiovascular adjustments are mainly due to CNS input to the baroreflex, thereby enhancing sympathetic neural activity.

Data used for this study included, for each subject, a 1 minute segment before each handgrip (baseline) and a 1 minute subsequent segment during handgrip with 30% of maximal voluntary contraction force (handgrip). Full details on this experimental protocol can be found in [61], [62].

D. Heartbeat Correction and Statistical Analysis

In order to provide reliable results, all RR-interval series must be free of algorithmic (*e.g.,* from automatic peak detection procedure) errors and ectopic beats in order to avoid potential biases in statistical outcomes. To eliminate such anomalies, we preprocessed all heartbeat data with a previously developed real-time R-R interval error detection and correction algorithm based on the point process statistics (local likelihood) [14]. Visual inspection analysis of all HRV series was also carried out.

All analyses were performed using the Matlab software suite. Concerning descriptive statistics, for every subject and for every feature (SAI, PAI, SAI/PAI, LF power, HF power, and LF/HF) we condensed the information about the time-varying dynamics of feature through its median across time. Then, for each feature, we evaluated between-group differences using bivariate non parametric statistics (Mann-Whitney or Wilcoxon test in case of unpaired or paired samples, respectively) under the null hypothesis that the between-subject medians of the two groups were equal.

Experimental results related to feature dynamics, presented in all of the figures and summary Tables below, are condensed as median and its respective standard error based on the median absolute deviation (MAD) across subjects/recordings. This is consistent with the Non-Gaussian distribution of some data samples ($p < 0.05$ from a Kolmogorov-Smirnov Normality test with null hypothesis of Gaussian distribution of data). Specifically, standard error was estimated as $1.4826\mathrm{MAD}(X)/\sqrt{n}$, where $\mathrm{MAD}(X) = \mathrm{Median}(|X - \mathrm{Median}(X)|)$, where X is the variable of interest (e.g., SAI, PAI, LF, HF, etc.), and n is the number of subjects in the dataset of interest.

A p-value of 0.05 was considered statistically significant.

VII. Experimental results

From each single ECG recording, the RR intervals were extracted using a curve length-based QRS detection algorithm [68]. Then, the resulting RR interval series was visually inspected and eventually corrected through a previously developed error detection and correction algorithm [14]. All recordings showed less than 5% of ectopic beats, and no significant algorithmic artifacts were detected.

The SAI-PAI validation was performed using the six experimental datasets described in Section VI. Beat-to-beat SAI-PAI estimates were derived from the double blockade dataset using Kalman filtering, whereas in all of the other datasets instantaneous SAI-PAI estimates with a 5ms temporal resolution were calculated using the point-process modeling. Full methodological details can be found in the Supplementary Materials.

In order to allow the reader to reproduce the methodology, in the following section generic Ψ values gathered from a multiple linear regression are reported using data from all of the available data/subjects undergoing autonomic blockade.

A. Working Model Coefficients Ψ_S and Ψ_P

Following are generalized values of sympathetic kernels Ψ_S gathered from multiple linear regression performed on data from all of the available data/subjects undergoing autonomic blockade (i.e., parasympathetic suppression), as well as parasympathetic kernels Ψ_P gathered from multiple linear regression performed on data from all of the available data/subjects undergoing autonomic blockade (i.e., sympathetic suppression).

The use of these coefficients, although with limited generality, is the first working attempt to estimate sympathetic and parasympathetic dynamics from ECG without the need of any calibration procedure at a single subject level.

Particularly, results reported in the following sections were obtained using the following realizations of Ψ_S and Ψ_P coefficients:

$$\Psi_S = \{39.2343, 10.1963, -5.9242\}$$
$$\Psi_P = \{28.4875, -17.3627, 5.8798, 12.0628, 5.6408, -7.0664, -5.6779, -3.9474\}$$

Considering also the standard deviation among realizations of Ψ_S and Ψ_P coefficients, statistical inference on healthy subjects is reported here (95% t-Student-based Confidence Interval):

TABLE I
Confidence Interval of Sympathetic and Parasympathetic Coefficients Ψ

	$j=0$	$j=1$	$j=2$	$j=3$	$j=4$	$j=5$	$j=6$	$j=7$
Ψ_{S_j}	39.2343±16.9821	10.1963±9.9895	-5.9242±6.0936	-	-	-	-	-
Ψ_{P_j}:	28.4875±11.4879	-17.3627±8.4911	5.8798±7.9916	12.0628±7.2923	5.6408±6.7928	-7.0664±4.8948	-5.6779±5.1945	-3.9474±5.8938

B. Validation 1: Tilt-table protocols

A first extensive validation was performed using data gathered from the tilt-table protocol, including stand-up, slow and fast tilting manoeuvres. Instantaneous estimates of all of the features were obtained using the point-process modeling with Laguerre expansion [7], [53]. To this extent, all KS plots and more than 98% of the autocorrelation samples fell within 95% confidence intervals, indicating that our modeling always provides a good characterization of the RR series, thus predicting heartbeats with satisfactory accuracy. Overall, KS distances were as low as 0.0220 ± 0.0056 (median $\pm$ MAD). Results from a comprehensive goodness-of-fit analysis are reported in the Supplementary Material.

Instantaneous estimates from a single subject are reported in Fig. 2. From this exemplary visual comparison between LF vs. SAI, HF vs. PAI, and LF/HF vs. SAI/PAI, it is of striking evidence how responses from the gravitational changes are clearly tracked at the individual level by the new indices (note the pattern corresponding to the red vertical lines indicating the postural transitions for SAI, PAI and SAI/PAI). Importantly, the old frequency band quantification has been effective at the group level, but (as clear from the figure) has never been able to work at the individual level. Results from other subjects confirm

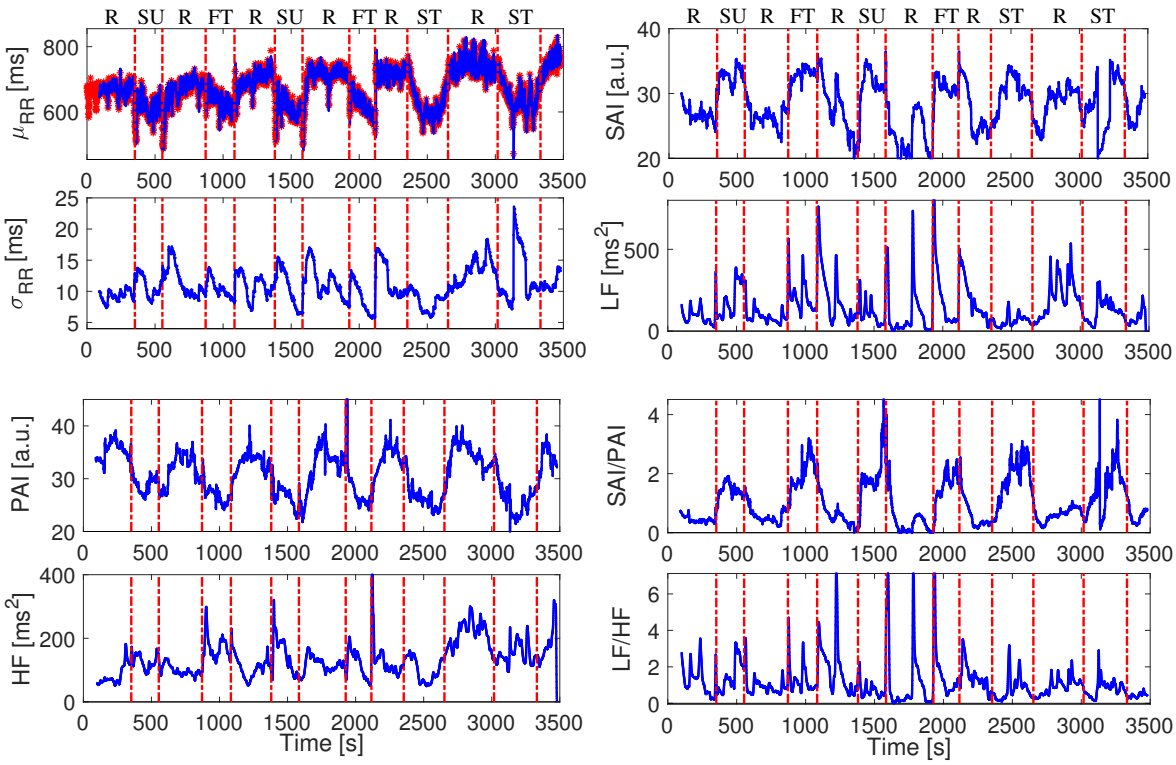

Fig. 2. Instantaneous heartbeat statistics computed from an exemplary subject of the Tilt-Table protocol. In the top-left panel, the estimated $\mu_{RR}(t)$, superimposed on the recorded R-R series, and the instantaneous heartbeat standard deviation $\sigma_{RR}(t)$ are shown. Instantaneous sympathetic and parasympathetic activity, and sympatho-vagal balance as estimated through SAI and PAI, and SAI/PAI ratio measures, along with the LF, HF and LF/HF ratio are shown in the other panels. Vertical dotted red lines indicate the beginning and end of each experimental transition. For this subject, the first transition is from rest (R) to stand-up (SU) and back, the second is from R to fast tilt (FT) and back, the third from R to SU, then R to FT, and the final two are from R to slow tilt (ST) and back.. Transitions are randomized for each subject.

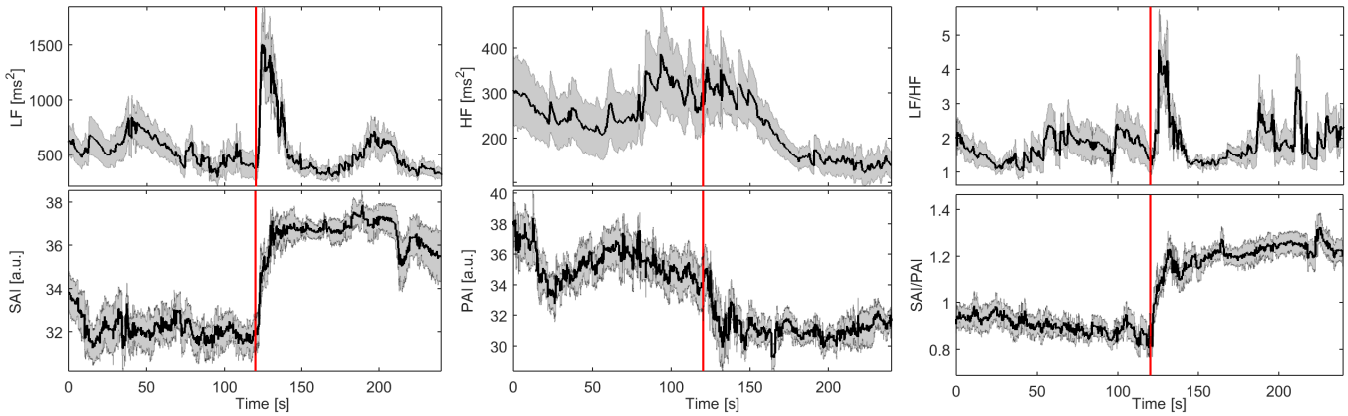

Fig. 3. TILT-TABLE PROTOCOL: FAST-TILT. Instantaneous point-process estimates averaged along all subjects, aligned with the transitions before and after fast-tilt. In the left panels the estimated instantaneous power $LF(t)$ and the SAI(t) can be compared. At each time, the median value is superimposed (black line) on the standard error of the median (gray area). Vertical red line indicates the beginning of the fast-tilt maneuver. Likewise, the estimated instantaneous power $HF(t)$ and the PAI(t) are shown in the central panels, whereas the estimated instantaneous $LF/HF(t)$ and the SAI/PAI(t) can be compared in the right panels.

this example, and a few more examples are reported in the Supplemental Material. Instantaneous series averaged among all subjects are shown in Figs. 3-5 aligned for each gravitational change: fast-tilt, slow-tilt, and stand-up. Several other instantaneous estimates at a single subject level are reported in the Supplementary Materials for further validation. Results give evidence that the proposed SAI and PAI measures, as well as the SAI/PAI ratio outperform the traditional autonomic characterization given by standard HRV instantaneous spectral analysis [7]. From the figures, it is possible to visually appreciate how the response from the proposed Sympathetic Activity Index (SAI), differently from the LF power, increases after gravitational stress (with a further delay after slow tilt) and remains at higher levels than the baseline session, thus reflecting sustained sympathetic activation. Conversely, the LF sharply increases with stimulation after fast tilt (Fig. 3), behaves erratically with stand up (Fig.

5), and even decreases after slow-tilt (Fig. 4), possibly mirroring vascular-related blood pressure dynamic responses. Note the sharper step responses tracked by the PAI index as compared with the HF measure.

Overall, we performed a comprehensive comparison of autonomic measures on the stand-up, slow, and fast tilt transitions including: standard estimates defined in the time and frequency domains from a traditional linear autoregressive model (AR); instantaneous standard estimates defined in the time and frequency domains from a traditional linear autoregressive point-process model (AR_{PP}) [7]; instantaneous standard estimates defined in the time and frequency domains from a linear autoregressive point-process model using the Laguerre expansion (ARL_{PP}) [53]; instantaneous SAI and PAI estimates from a point-process model having the kernels, Ψ_S and Ψ_P, calculated through:

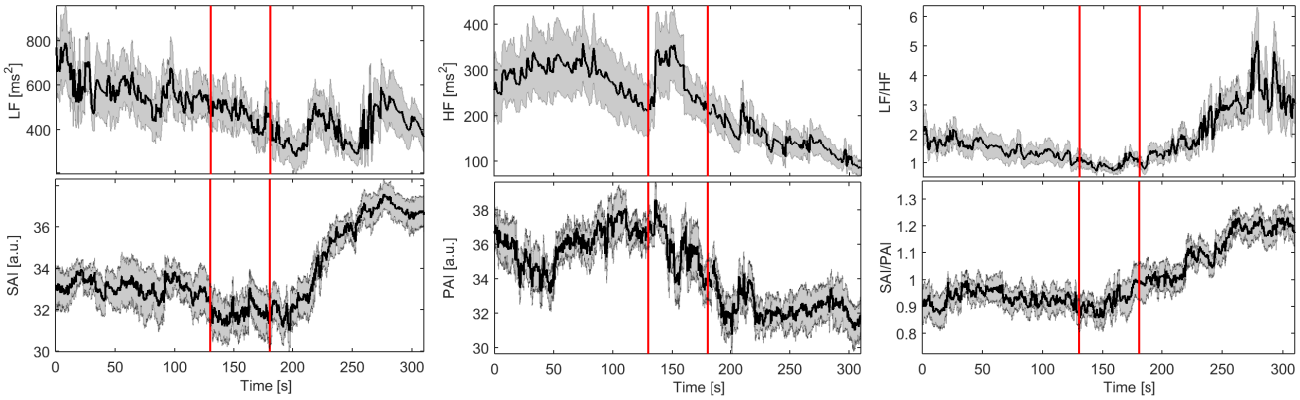

Fig. 4. TILT-TABLE PROTOCOL: SLOW-TILT. Instantaneous point-process estimates averaged along all subjects, aligned with the slow-tilt transitions. In the left panel, the estimated instantaneous power $LF(t)$ and the SAI(t) can be compared. At each time, the median value is superimposed (black line) on the standard error of the median (gray area). The two vertical red lines indicate the start and end of the slow tilting manoeuver. Likewise, the estimated instantaneous power $HF(t)$ and the PAI(t) can be compared in the central panels, whereas the estimated instantaneous $LF/HF(t)$ and the SAI/PAI(t) can be compared in the right panels.

- NEW(0): a multiple linear regression using subject specific (*i.e.* performed for each subject) recording from one rest-upright condition;
- NEW(1): a multiple linear regression using subject specific (*i.e.* performed for each subject) recording averaging Ψ_S and Ψ_P estimates from stand-up, slow and fast tilting conditions.
- NEW(2): a multiple linear regression using general values (*i.e.* calculated over all of the subjects), averaging Ψ_S and Ψ_P estimates from stand-up, slow and fast tilting conditions, following a leave one subject out procedure.
- NEW(3): a multiple linear regression using general values (*i.e.* calculated over all of the subjects) averaging Ψ_S and Ψ_P estimates from the rest-tilt control session of an independent dataset.
- NEW(4): a multiple linear regression using general values (*i.e.* calculated over all of the subjects) averaging Ψ_S and Ψ_P from subjects of an independent dataset undergoing autonomic blockade (parasympathetic suppression $\rightarrow$ sympathetic kernels Ψ_S; sympathetic suppression $\rightarrow$ parasympathetic kernels Ψ_P. See Section V for details.)

Standard HRV measures, *i.e.* RMSSD, pNN50(%), HRV triangular index (HRV_tri_ind), and TINN, are also calculated and reported.

Numerical results using the NEW(4) estimation method are shown in Tables II, III, and IV. All other results are included in the Supplementary Materials.

Concerning sympathetic activity, results show that SAI estimates are always able to effectively discern between resting and upright conditions. Using Ψ_S and Ψ_P kernels of general applicability, increased sympathetic activity after stand-up is significantly revealed, with $p < 4 \cdot 10^{-5}$, as well as after slow tilt ($p < 0.007$) and fast tilt $p < 9 \cdot 10^{-4}$. No significant results are reported using indices of LF power ($p > 0.05$). Likewise, for parasympathetic activity, results show that PAI estimates are always able to effectively discern between resting and upright conditions. Using Ψ_S and Ψ_P kernels of general applicability, decreased parasympathetic activity after stand-up was revealed with $p < 6 \cdot 10^{-4}$, as well as after slow tilt ($p < 0.011$) and fast tilt ($p < 0.002$). Significant results are achieved using indices of HF power, as estimated through standard AR modeling on the slow tilt ($p < 0.03$). Statistical analysis for all other indices yielded no significant results ($p > 0.05$). Finally, group-wise statistics of sympatho-vagal balance show that SAI/PAI estimates were always able to effectively discern between resting and upright conditions. Using Ψ_S and Ψ_P kernels of general applicability, increased sympatho-vagal balance after stand-up was revealed with $p < 4 \cdot 10^{-6}$, as well as after slow tilt ($p < 0.001$) and fast tilt ($p < 2.629 \cdot 10^{-4}$). No significant results were achieved using indices of LF/HF ratio ($p > 0.05$).

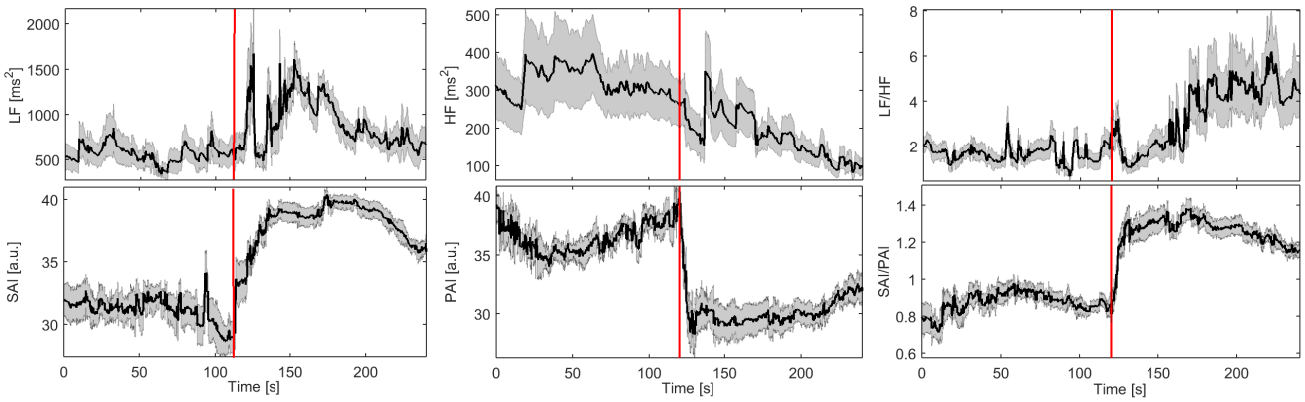

Fig. 5. TILT-TABLE PROTOCOL: STAND UP. Instantaneous point-process estimates averaged along all subjects, aligned with the stand-up transitions. In the left panels, the estimated instantaneous power $LF(t)$ and the SAI(t) can be compared. At each time, the median value is superimposed (black line) on the standard error of the median (gray area). Vertical red lines indicate the beginning of the stand-up maneuver. Likewise, the estimated instantaneous power $HF(t)$ and the PAI(t) can be compared in the central panels, whereas the estimated instantaneous $LF/HF(t)$ and the SAI/PAI(t) can be compared in the right panels.

TABLE II
RESULTS FROM THE REST - STAND UP EXPERIMENTAL DATASET

	Autonomic Index	Rest	Stand-Up	p-value
	LF	516.16 ± 311.31	152.33 ± 379.46	0.270000
Sympathetic Activity	SAI	30.03 ± 3.17	39.05 ± 2.05	0.000031
	HF	337.17 ± 247.07	155.23 ± 73.60	0.408000
Parasympathetic Activity	PAI	35.91 ± 1.84	29.63 ± 3.25	0.000570
	LF/HF	1.88 ± 1.36	3.25 ± 2.59	0.242000
Sympatho-Vagal Balance	SAI/PAI	0.85 ± 0.14	1.29 ± 0.13	0.000003

p-values are obtained from the rank-sum test between the Rest and Stand-up sessions.

TABLE III
RESULTS FROM THE REST - SLOW TILT-TABLE EXPERIMENTAL DATASET

	Autonomic Index	Rest	Titl-Table Slow	p-value
	LF	552.42 ± 388.69	368.13 ± 220.38	0.715000
Sympathetic Activity	SAI	33.50 ± 3.17	36.05 ± 1.59	0.007000
	HF	295.12 ± 192.60	128.92 ± 77.27	0.060000
Parasympathetic Activity	PAI	36.42 ± 2.92	31.96 ± 3.15	0.011000
	LF/HF	1.39 ± 1.071	3.00 ± 1.43	0.126000
Sympatho-Vagal Balance	SAI/PAI	0.95 ± 0.13	1.15 ± 0.13	0.001000

p-values are obtained from the rank-sum test between the Rest and Slow-Tilt sessions.

TABLE IV
RESULTS FROM THE REST - FAST TILT-TABLE EXPERIMENTAL DATASET

	Autonomic Index	Rest	Titl-Table Fast	p-value
	LF	568.28 ± 299.64	504.37 ± 269.77	0.704000
Sympathetic Activity	SAI	31.80 ± 2.21	36.79 ± 1.85	0.000870
	HF	239.12 ± 177.12	203.04 ± 102.98	0.815000
Parasympathetic Activity	PAI	35.89 ± 2.95	30.62 ± 1.58	0.002000
	LF/HF	1.82 ± 1.43	1.56 ± 0.65	0.977000
Sympatho-Vagal Balance	SAI/PAI	0.87 ± 0.13	1.21 ± 0.13	0.000263

p-values are obtained from the rank-sum test between the Rest and Fast-Tilt sessions.

C. Validation 2: Lower Body Negative Pressure

A second validation of our SAI-PAI estimates was performed using data gathered from the Lower Body Negative Pressure (LBNP) protocol. Instantaneous estimates of all of the features were obtained using point-process modeling with Laguerre expansion [7], [53]. All KS plots but 3, and more than 98% of the autocorrelation samples fell within 95% confidence intervals, indicating a very good fit. Considering all the 108 recordings, KS distances were as low as 0.0366 ± 0.0082 (Median $\pm$ MAD). Results from a comprehensive goodness of fit analysis are reported in the Supplementary Material. Instantaneous series averaged among all 58 subjects are shown in Fig. 6. Results of the statistical comparison are reported in Tab. V. From the figure, it is possible to visually appreciate how the proposed Sympathetic Activity Index (SAI), differently from the LF power, increases after gravitational stress by tracking a clear exponential-like step response, thus reflecting sustained sympathetic activation. Conversely, the LF sharply increases with stimulation right after the step pressure change, and then behaves erratically along time. Also here, note the sharper step responses tracked by the PAI index as compared with the HF measure.

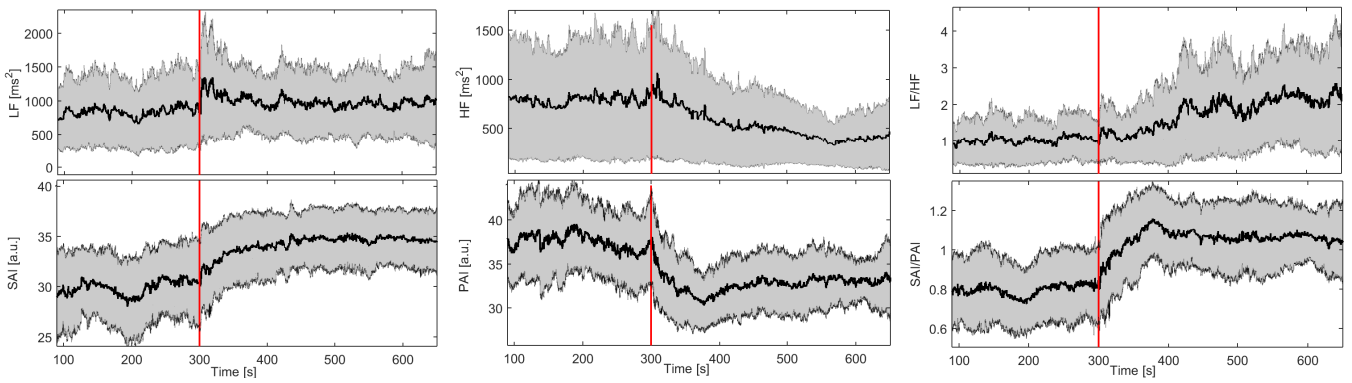

Fig. 6. LBNP PROTOCOL. Instantaneous point-process estimates averaged along all subjects, aligned with the LBNP transitions. In the left panel the estimated instantaneous power $LF(t)$ and the SAI(t) are shown. At each time, the median value is superimposed (black line) on the standard error of the median (gray area). Vertical red line indicates the beginning of the LBNP maneuver. Likewise, the estimated instantaneous power $HF(t)$ and the PAI(t) are shown in the central panel, whereas the estimated instantaneous $LF/HF(t)$ and the SAI/PAI(t) are shown in the right panel.

TABLE V
COMPARISON OF AUTONOMIC INDICES BETWEEN REST AND LBNP.

Autonomic Index	**Rest**	**LBNP**	**p-value**
LF [ms^2]	875.530 $\pm$ 525.734	964.204 $\pm$ 402.282	0.440
*SAI [a.u.]	29.890 $\pm$ 3.828	34.353 $\pm$ 2.708	$3.950{\cdot}10^{-16}$
*HF [ms^2]	766.415 $\pm$ 602.566	457.434 $\pm$ 324.865	$9.248{\cdot}10^{-8}$
*PAI [a.u.]	38.218 $\pm$ 3.586	32.647 $\pm$ 2.712	$1.665{\cdot}10^{-12}$
*LF/HF	1.043 $\pm$ 0.578	1.542 $\pm$ 0.878	$1.614{\cdot}10^{-8}$
*SAI/PAI	0.774 $\pm$ 0.146	1.067 $\pm$ 0.151	$7.496{\cdot}10^{-16}$

p-values from the signrank non-parametric test for paired data.
* indicates significant differences between Rest and LBNP sessions.

It should be noted that, based on the p-values for this paradigmatic case, the proposed SAI and PAI measures, as well as the SAI/PAI ratio, outperform the traditional autonomic characterization given by standard HRV instantaneous spectral analysis [7]. Once again, the increase of sympathetic activity as identified by the SAI index presents a slower time constant than the parasympathetic one, which is identified by the PAI index.

Concerning sympathetic activity, results show that SAI estimates are able to effectively identify expected increases during LBNP conditions with respect to resting state with $p < 5 \cdot 10^{-16}$, despite no significant statistics were obtained through indices of LF power ($p > 0.05$).

Moreover, expected decreases in parasympathetic activity during LBNP are effectively revealed through PAI estimates with $p < 2 \cdot 10^{-12}$, as well as indices of HF power ($p < 10^{-8}$), whereas increases in the sympatho-vagal balance during LBNP are identified through SAI/PAI estimates with $p < 8 \cdot 10^{-16}$, as well as indices of LF/HF ratio ($p < 2 \cdot 10^{-8}$).

D. Validation 3: Handgrip

A further validation of our SAI-PAI estimates was performed using data gathered from the handgrip protocol. Instantaneous estimates of all of the features were obtained using point-process modeling with Laguerre expansion [7], [53]. All KS plots but 7, and more than 98% of the autocorrelation samples fell within 95% confidence intervals, indicating a very good fit. Considering all 108 recordings, KS distances were as low as 0.0647 ± 0.0102 (Median $\pm$ MAD). Results from a comprehensive goodness of fit analysis are reported in the Supplementary Material. Instantaneous series from all subjects are shown in Fig. 7. Results of the statistical comparison are reported in Tab. VI.

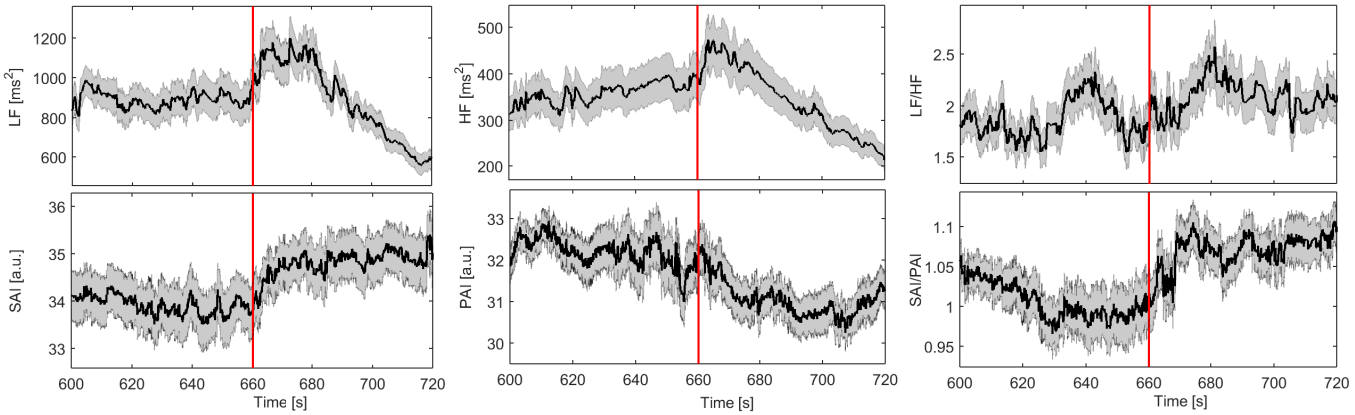

Fig. 7. HANDGRIP PROTOCOL. Instantaneous point-process estimates averaged along all subjects, aligned with the handgrip transitions. In the left panel the estimated instantaneous power $LF(t)$ and the SAI(t) are shown. At each time, the median value is superimposed (black line) on the standard error of the median (gray area). Vertical red line indicates the beginning of the handgrip task. Likewise, the estimated instantaneous power $HF(t)$ and the PAI(t) are shown in the central panel, whereas the estimated instantaneous $LF/HF(t)$ and the SAI/PAI(t) are shown in the right panel.

TABLE VI
COMPARISON OF AUTONOMIC INDICES BETWEEN BASELINE AND HANDGRIP

Autonomic Index	Baseline	Handgrip	p-value
LF [ms^2]	982.257 $\pm$ 579.178	924.135 $\pm$ 479.580	0.135
*SAI [a.u.]	34.569 $\pm$ 2.946	35.719 $\pm$ 3.022	0.006
*HF [ms^2]	414.418 $\pm$ 324.917	416.781 $\pm$ 332.342	0.009
*PAI [a.u.]	33.055 $\pm$ 2.979	31.527 $\pm$ 2.744	0.002
LF/HF	2.059 $\pm$ 1.438	2.465 $\pm$ 1.636	0.302
*SAI/PAI	1.052 $\pm$ 0.179	1.130 $\pm$ 0.153	$8.584{\cdot}10^{-4}$

p-values from the signrank non-parametric test for paired data
* indicates significant differences between Rest and LBNP sessions.

Once again, the proposed SAI and PAI measures, as well as the SAI/PAI ratio, outperform the traditional autonomic characterization given by standard HRV instantaneous spectral analysis [7]. The increase in sympathetic activity during the handgrip task, with respect to baseline, is effectively identified by the SAI index, both visually (Fig.6) and with statistical significance ($p < 0.006$). No significant statistics are reported through indices of LF power ($p > 0.05$).

Furthermore, decreases in parasympathetic activity during handgrip are effectively revealed through PAI estimates with $p < 0.002$, as well as indices of HF power ($p < 0.009$), whereas increases in sympatho-vagal balance during handgrip are identified through SAI/PAI estimates exclusively, with $p < 9 \cdot 10^{-4}$. No significant statistics are obtained through LF/HF ratio indices ($p > 0.05$).

VIII. DISCUSSION AND CONCLUSION

Despite widespread use during the last two decades, HRV analyses based on frequency domain techniques have faced significant challenges in assessing cardiac autonomic activity [17], [19], [39]. Several pharmacological studies have confirmed the intrinsic ambiguity of this approach, as HRV-related changes below 0.15 Hz are mediated by both cardiac vagal and sympathetic nerves [9], [23], [24], [41]. In addition, changes in the LF power of HR variability often occur in response to arterial blood pressure fluctuations, which cause HR fluctuations through the baroreflex [2]. A variety of sophisticated methodologies have been proposed to address these issues [10], [58], [59], [63], [64], [66], [67]. However, their impact in cardiovascular research has been limited due to methodological (e.g., stationarity, the need of a broadband HR spectrum) or practical shortcomings (e.g., the need of multivariate autonomic recordings such as ECG and respiration). The issues are even more challenging for clinical monitoring, where relatively rudimentary concepts and simple computational algorithms for

HRV analysis have been used for clinical monitoring. Moreover, using HRV spectra, several commercially available mobile applications have not been able to provide precise, reliable assessments of stress levels, sleep quality, or recovery from athletic activity [49], [60]. These shortcomings in current autonomic measures are due in part to high inter-individual variability. Current techniques have not been accurate enough to provide meaningful autonomic measures that are valid for group analysis, while simultaneously being tailored to the individual subject, particularly for sympathetic activity.

This manuscript introduces a set of autonomic measures which differ from those used previously. PAI and SAI provide: 1) independent parasympathetic and sympathetic dynamics, 2) exclusively use heartbeat intervals, 3) can be computed continuously in real time without concerns of stationarity, and 4) appear to be reliable for both group and individual assessment. The novel identification procedure is a simple non-trivial way to calculate non-invasive, time-resolved autonomic markers having features of effectiveness, reliability, and high resolution in time. Importantly, the metrics offer the potential to continuously track cardiac autonomic control in both clinical and research settings. The methodology is also applicable to any sequence of heartbeat events - e.g. ECG, echocardiographic parameters, arterial pressure parameters, video signals, ballistogram, ultra wideband cardiogram etc. The time-varying estimates of SAI and PAI were shown to provide instantaneous features consistent with a wide range of individual subject's conditions in a variety of autonomic states. Several estimation techniques can be used to obtain beat-to-beat or finite estimates in time using, e.g., Kalman or least square methods, respectively. In addition, instantaneous SAI and PAI estimates can be obtained through point-process modeling [7], [53].

These novel measures were validated using datasets collected in controlled physiological conditions, and involving well-known sympatho-vagal changes, including: orthostatic changes from standing; slow tilting and fast tilting; autonomic blockade during postural changes; lower body negative pressure; and handgrip. In all the cases evaluated, the results of the new technique demonstrated superiority at separating the sympathetic and parasympathetic components using the SAI and PAI signals, as compared to existing methods.

By using comprehensive inter-subject statistics computed every 5 ms, the SAI index correctly demonstrated the expected increases of sympathetic activation and vagal withdrawal in all the autonomic scenarios that have been tested. The analyses are scientifically thorough with time-varying estimates, avoiding the loss of information inherent in the static metrics typically reported in the literature. The results were also compared to three different reported methodologies: 1) a simple window-based autoregressive model demonstrating comparison to the published HRV guidelines [47], 2) a time-varying point-process autoregressive model providing a comparison which accounts for nonstationary [7], and 3) a time-varying point-process model using Laguerre functions [53]. For assessment of sympathetic and parasympathetic activity, SAI, PAI, and SAI/PAI appear to track expected physiological responses much more closely than LF, HF or LF/HF in all the datasets evaluated. The new parameters showed particular improvement in inter-subject variability, reflected in lower standard errors, and more significant difference in the statistical comparisons (see details in Tables VIII, IX, and X).

Importantly, the SAI and PAI measures are derived in a non-obvious and original way. Although the methodological framework may share relevant features adopted in the past, such as the use of Laguerre expansion [5], the derivation is the first attempt at proposing a proper combination of coefficients derived by Laguerre functions, which yield very specific features in the time and frequency domains [32], [34], [53]. It is also noteworthy that once a standard autoregressive model has been identified along the Laguerre bases (i.e. after convolving the original RR interval series with the Laguerre bases), the use of SAI and PAI measures does not need calibration. The derivation of pre-estimated kernels of general applicability for the SAI and PAI estimation take of data gathered from selective sympathetic and parasympathetic blockade.

The overall approach stems from the intuitive hypothesis that the cholinergic and adrenergic systems have different temporal dynamics which overlap in the frequency domain. Thus, a proper weighted sum and/or subtraction of primitives derived from orthonormal Laguerre bases is able to reflect the actual autonomic activity, disentangling the specific sympathetic and parasympathetic contributions. In the frequency domain, for a given α, the spectra of Laguerre functions have equal magnitude and different phase spectra. The classic HRV analysis is limited by the pre-defined frequency ranges (VLF, LF and HF) , whereas the Laguerre functions do not define a space in the frequency domain but constitute a set of mathematical functions characterizing a specific fine modulation of the number of oscillations across zero, as well as very specific time responses.

An important limitation of the study is that the identification of kernels of general applicability has been performed using data coming from a limited number of subjects. Consequently, non-parametric paired comparisons using data from selective parasympathetic and sympathetic blockade resulted in non-significant p-values; however, central trends were as expected. Although an extensive validation was performed of the proposed SAI and PAI through more than 230 ECG recordings, all the data was from healthy volunteers. Therefore, it cannot be excluded that a more accurate identification of Ψ_S and Ψ_P kernels of general applicability may be necessary when dealing with data from subjects with various cardiovascular pathologies or subjects with peculiar heartbeat dynamics (e.g., infants and newborns). Likewise, it cannot be excluded that the Ψ_S and Ψ_P kernels estimation could be improved by considering cases where subjects elicit peculiar respiratory patterns. Also, the absolute value of SAI and PAI estimates is currently dependent on the arbitrary ranges chosen for the fitting procedure described in paragraph V-A. A proper study on the scalability of SAI and PAI estimates should be performed in order to obtain normalized indices with improved interpretability. Finally, depending on the estimation method used to identify the Laguerre coefficients, the initial part of the recording is left without actual SAI and PAI estimates because the point-process modeling needs at least the first 70 s of ECG must be used for model initialization [7], [53]. There is also likely room to improve the proposed identification using

data from a more diverse pool of subjects undergoing selective autonomic blockade while undergoing significant orthostatic changes. Moreover, given the ability of our model to characterize the probabilistic structure of RR intervals generation as related to mean heart rate, future studies might consider more detailed analyses on the relationship between these two variables as linked to other cardiovascular correlates (e.g., respiration, blood pressure, etc.). Future studies might include a variety of different manipulations of cardiovascular control.

Despite the above limitations, the strength of the algorithm lies in estimating SAI-PAI values through an appropriate combination of orthonormal Laguerre bases. When applied to physiological data, there has been strong statistical support for demonstrating changes in sympatho-vagal balance in all the experimental settings. Note that the proposed framework has been particularly successful in significantly reducing inter-subject variability with respect to HRV frequency domain analysis. These improvements enhance the statistical power of the SAI and PAI measures when compared with standard measures using LF and HF powers (in some instances by as much as 10^{16}).

By definition, SAI and PAI are dimensionless numbers. Moreover, SAI and PAI estimates are relative to “reference levels" of sympathetic and parasympathetic activity during supine resting state, and upright position after postural change. By definition, the actual value of such “reference levels" is arbitrary, as long as prior constraints from physiological dynamics are taken into account (dominant parasympathetic activity during supine resting state, dominant sympathetic activity during upright position after postural change).

From a methodological point of view, extension of the SAI-PAI derivation with nonlinear modeling could open new avenues for the estimation of sympathetic and parasympathetic nonlinear dynamics, as well as effective quantification of nonlinear sympathetic-parasympathetic interactions, which may be based on bi-spectral and other higher order spectral analyses. There are a variety of major clinical and non-clinical applications using SAI-PAI estimates. Finally, since the SAI and PAI measures are derived from heartbeats exclusively, so it is possible to calculate them through any portable, possibly wearable device carrying heart beat event information.

ACKNOWLEDGEMENTS

Authors are grateful to Roger G. Mark and Thomas Heldt (Harvard-MIT Division of Health Sciences and Technology, Cambridge, MA, USA) for kindly providing the tilt-table data, and to Vegard Bruun Wyller (Rikshospitalet University Hospital, Oslo, Norway) for kindly providing the lower body negative pressure and handgrip data analyzed in this study. This study received partial funding from the Department of Anesthesia, Critical Care and Pain Medicine, Massachusetts General Hospital, Harvard Medical School, Boston, MA, USA.

DISCLOSURE OF CONFLICT OF INTEREST

An International Application (PCT/US2016/044844) was filed on 29.07.16 for the method described in this paper.

SUPPLEMENTARY MATERIAL / APPENDIX

Autoregressive models and Laguerre Expansion

Let us consider a general formulation of a Autoregressive Model (AR):

$$y(k) = \mathbf{F}(y(k-1), y(k-2), ..., y(k-M)) + \epsilon(k). \tag{5}$$

By taking into account a linear combination of the past events, the AR model can be can be written as following:

$$y(k) = \gamma_0 + \sum_{i=1}^{M} \gamma_1(i) y(k-i) + \epsilon(k). \tag{6}$$

where $\epsilon(k)$ are independent, identically distributed Gaussian random variables and M is the memory of the model. Due to the autoregressive structure of (6), the system can be identified with only exact knowledge of the output data and with only few assumptions on the input data. To improve the system identification process (i.e. γ_0, γ_1 estimations) and to reduce the number of required parameters, it is possible to expand the AR kernels by means of orthonormal bases. A widely used expansion uses the Laguerre functions [32], [34], [53]. Specifically, let define the j^{th}-order discrete time orthonormal Laguerre function (see fig. 8):

$$\phi_j(k) = \alpha^{\frac{k-j}{2}} (1-\alpha)^{\frac{1}{2}} \sum_{i=0}^{j} (-1)^i \binom{k}{i} \binom{j}{i} \alpha^{j-i} (1-\alpha)^i, \ (k \geq 0)$$

where α is the discrete-time Laguerre parameter ($0 < \alpha < 1$) which determines the rate of exponential asymptotic decline of these functions.

Given the Laguerre function, $\phi_j(k)$, and the signal, $y(k)$, the j^{th}-order Laguerre filter output is:

$$l_j(k) = \sum_{i=0}^{\infty} \phi_j(i)\, y(k-i-1) \tag{7}$$

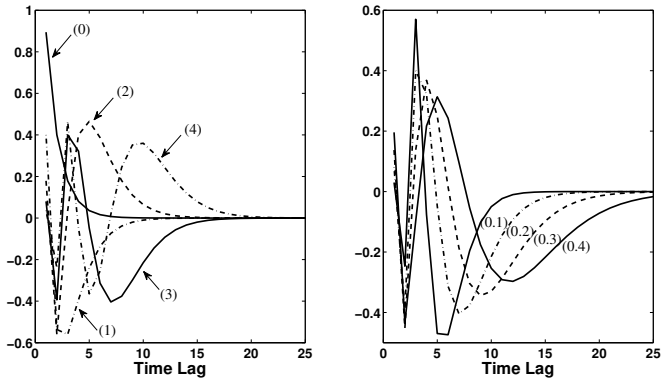

Fig. 8. (Left) First 4 Laguerre Functions for $\alpha = 0.2$ plotted over the first 25 lags. The order of each Laguerre basis is indicated under brackets. (Right) The 3^{rd} Laguerre functions for $\alpha = 0.1, 0.2, 0.3, 0.4$. The corresponding α value is indicated under brackets.

The computation of the Laguerre Filter output can be accelerated significantly by use of the following recursive relation [32], [34], [53]:

$$l_0(k) = \sqrt{\alpha}\, l_0(k-1) + \sqrt{1-\alpha}\, y(k-1) \tag{8}$$

$$l_j(k) = \sqrt{\alpha}\, l_j(k-1) + \sqrt{\alpha}\, l_{j-1}(k) + \tag{9}$$

$$\sqrt{\alpha}\, l_{j-1}(k-1),\ j \geq 1 \tag{10}$$

Since the $\{\phi_i(t)\}$ form a complete orthonormal set in functional space $\mathcal{L}_2$, we can write [42]:

$$\gamma_0 = g_0 \tag{11}$$

$$\gamma_1(i) = \sum_{j=0}^{P} g_1(j)\phi_j(i)\ . \tag{12}$$

Here g_0, and $g_1(j)$ are constant coefficients. The expansion goes to zero as i goes to infinity. Using (7) and (11)–(12), the model in eq. 6 becomes:

$$y(k) = g_0 + \sum_{j=0}^{P} g_1(j)\, l_j(k) + \epsilon(k)\ . \tag{13}$$

hereinafter called Autoregressive with Laguerre expansion (ARL) model. The number of parameters to estimate is $N = 1 + (P+1)$. Although the Laguerre filters have infinite memory, the AR model corresponding to the ARL representation can be truncated to an order M which depends on how fast the Laguerre functions decade to zero. It is also noteworthy that when $\alpha = 0$ the filter output becomes $l_j(k) = (-1)^j y(k-j-1)$ and the ARL model corresponds to the AR model apart for the sign.

Time-varying implementation

The iterative estimation along time of the novel SAI-PAI measures can be performed using several signal processing methods. For example, a simple Kalman filtering can be used to track the SAI-PAI dynamics at each heartbeat, whereas an instantaneous estimation (i.e., at each moment in time) can be performed using the point-process modeling. Of note, traditional recursive least-square and window-based methods can also be applied.

Heartbeat Interval Point-Process Model : A random point process is a stochastic process which can be thought of as registering the occurrence in time of discrete events [4]. Point process theory has been widely used in modeling various types of random events (e.g., eruptions of earthquakes, queueing of customers, spiking of neurons, etc.) where the timing of the events are of central interest. Bearing a similar spirit, the point process theory has been used for modeling human heartbeats [7], [12], [51]–[54]. The point process framework primarily defines the probability of having a heartbeat event at each moment in time (see Figure 9).

A parametric formulation of the probability function allows for a systematic, parsimonious estimation of the parameter vector in a recursive way and at any desired time resolution. Instantaneous indexes can then be derived from the parameters in order to quantify important features as related to cardiovascular control dynamics. Mathematically, let $(0, T]$ denote the observation interval and $0 \leq u_1 < \cdots < u_k < u_{k+1} < \cdots < u_K \leq T$ the times of the events. For $t \in (0, T]$, let $N(t) = \max\{k : u_k \leq t\}$ be the sample path of the associated counting process. Its differential, $dN(t)$, denotes a continuous-time indicator function,

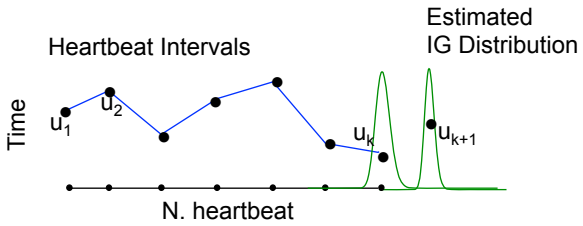

Fig. 9. A graphical representation of point-process modeling of heartbeat dynamics. The horizontal axis represents the counting process along the number of heartbeats, whereas the vertical axis represents the duration of heartbeat intervals. Inverse-Gaussian (IG) distributions (green lines on the right) characterize the prediction of the future heartbeat event along the time (from [55]).

where $dN(t) = 1$, when there is an event (such as the ventricular contraction) or $dN(t) = 0$, otherwise. Let define also a left continuous function $\widetilde{N}(t) = \lim_{\tau \to t^-} N(\tau) = \max\{k : u_k < t\}$ which will be useful in the following definitions.

By treating the R-waves as discrete events, we may develop a point process probability model in the continuous time domain [7]. Assuming history dependence, the probability density of the waiting time $t–u_j$ until the next R-wave event follows an inverse Gaussian model:

$$f(t|\mathcal{H}_t, \xi(t)) = \left[\frac{\xi_0(t)}{2\pi(t-u_j)^3}\right]^{\frac{1}{2}} \exp\left\{-\frac{1}{2}\frac{\xi_0(t)[t-u_j-\mu_{RR}(t,\mathcal{H}_t,\xi(t))]^2}{\mu_{RR}(t,\mathcal{H}_t,\xi(t))^2(t-u_j)}\right\} \tag{14}$$

where $j = \widetilde{N}(t)$ denotes the index of the previous R-wave event occurred before time t, $\mathcal{H}_t = (u_j, RR_j, RR_{j-1}, ..., RR_{j-M+1})$,$\xi(t)$ is the vector of the time-varing parameters, $\mu_{RR}(t, \mathcal{H}_t, \xi(t))$ represents the first-moment statistic (mean) of the distribution, and $\xi_0(t) = \theta > 0$ denotes the shape parameter of the inverse Gaussian distribution, (as $\theta/\mu \to \infty$, the inverse Gaussian distribution converges to a Gaussian distribution). The function $f(t|\mathcal{H}_t, \xi(t))$ indicates the probability of having a beat at time t given that a previous beat has occurred at u_j and $\mu_{RR}(t, \mathcal{H}_t, \xi(t))$ can be interpreted as signifying the prediction of the time when the next beat is expected to occur. By definition, $f(t|\mathcal{H}_t, \xi(t))$ is characterized at each moment in time, at the beat as well as in-between beats.

The use of an inverse Gaussian distribution to characterize the R-R intervals occurrences is motivated by the fact that if the rise of the membrane potential to a threshold initiating the cardiac contraction is modeled as a Gaussian random walk with drift, then the probability density of the times between threshold crossings (the R-R intervals) is indeed the inverse Gaussian distribution [7]. In [11], we have compared heartbeat interval fitting point process models using different probability distributions, and found that the inverse Gaussian model achieved the overall best fitting results. The parameter $\mu_{RR}(t, \mathcal{H}_t, \xi(t))$ denotes the instantaneous R-R mean that can be modeled as a generic function of the past (finite) R–R values $\mu_{RR}(t, \mathcal{H}_t, \xi(t)) = g(RR_{\widetilde{N}(t)}, RR_{\widetilde{N}(t)-1}, ..., RR_{\widetilde{N}(t)-h+1})$, where $RR_{\widetilde{N}(t)-j+1}$ denotes the previous j^{th} R–R interval occurred prior to the present time t. In our previous work [6], [11], the history dependence is defined by expressing the instantaneous mean $\mu_{RR}(t, \mathcal{H}_t, \xi(t))$ as a linear combination of present and past R-R intervals (in terms of an AR model), i.e., function g is linear.

Concerning the parameter estimation, we used a Newton-Raphson procedure to maximize the local log-likelihood and compute the local maximum-likelihood estimate of $\xi(t)$ [7], [53] within $W = 90s$. Because there is significant overlap between adjacent local likelihood intervals, we started the Newton-Raphson procedure at t with the previous local maximum-likelihood estimate at time $t - \delta$ in which δ defines how much the local likelihood time interval is shifted to compute the next parameter update. The model goodness-of-fit is based on the Kolmogorov-Smirnov (KS) test and associated KS statistics (see details in [7], [53]). Autocorrelation plots were considered to test the independence of the model-transformed intervals [7], [53]. Once the model order is determined, the initial model coefficients were estimated by the method of least squares [7], [53].

Block schemes

Block schemes of all the stages involved in the SAI-PAI estimation are described in Figs 10 and 11. A modeling stage has been devised in order to establish the combination and structure of the base functions attributed either to the sympathetic or parasympathetic activity. On a real set of heartbeats, given such a modeling structure as specified in eq. 1, the estimation of model-defined parameters (g_{1s}, g_{1p}) can be updated along the time using the most efficient and popular methods reported in the literature for recursive parameter estimation (Kalman filtering, point processes, recursive least square, etc.). A final step linearly combines the time-varying estimation using the disentangling coefficients Ψ_s, Ψ_p to yield the final SAI and PAI measures. The block scheme reported in Fig. 11 has to be considered as an in-depth look of the block “Modeling and Multiple Regression" in Fig. 10. Here, heartbeat data gathered during sympathetic activity only (parasympathetic blockade), and during sympathetic activity only (parasympathetic blockade) both in a supine resting phase and a standing tilting phase were considered as reference heartbeat data. For each of these datasets, after fitting an AR model with Laguerre expansion of the terms, a multiple regression stage considering desired changes (e.g., increase of the sympathetic activity during tilt with

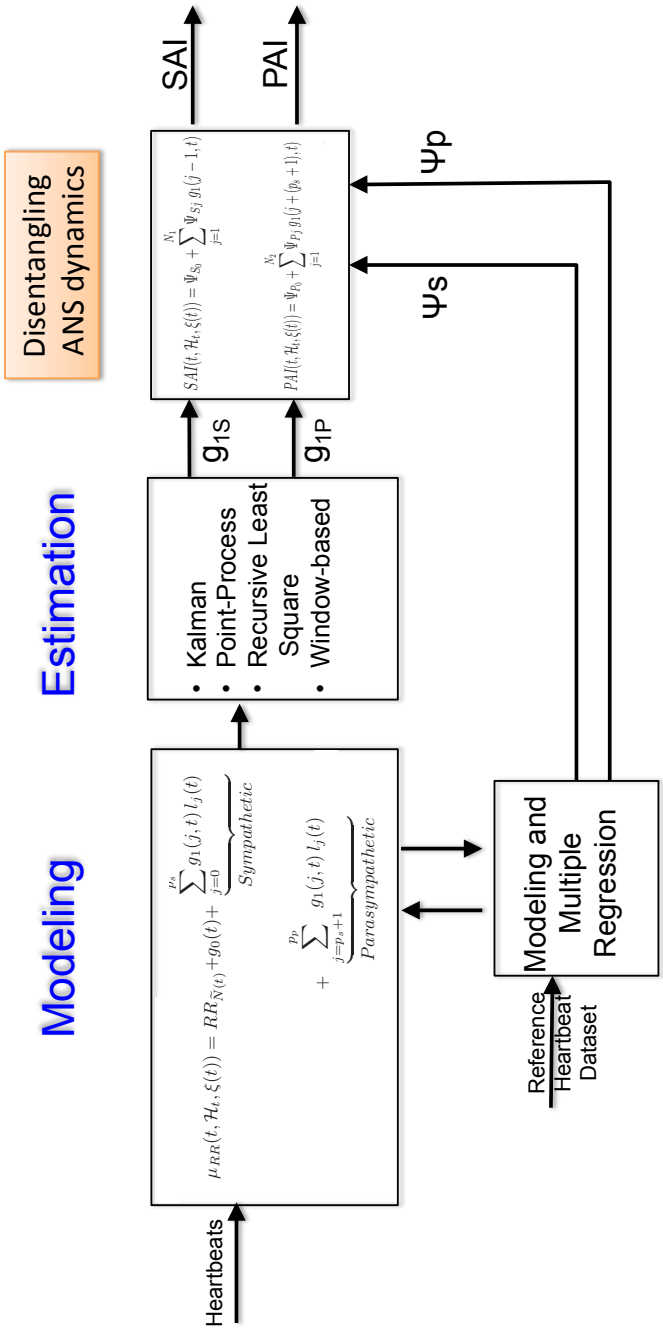

Fig. 10. Block scheme of the modeling and estimation stages involved in the SAI-PAI calculation.

respect to rest) has been performed for each subject. Then, coefficients of general applicability Ψ_s, Ψ_p were obtained through the average among subjects.

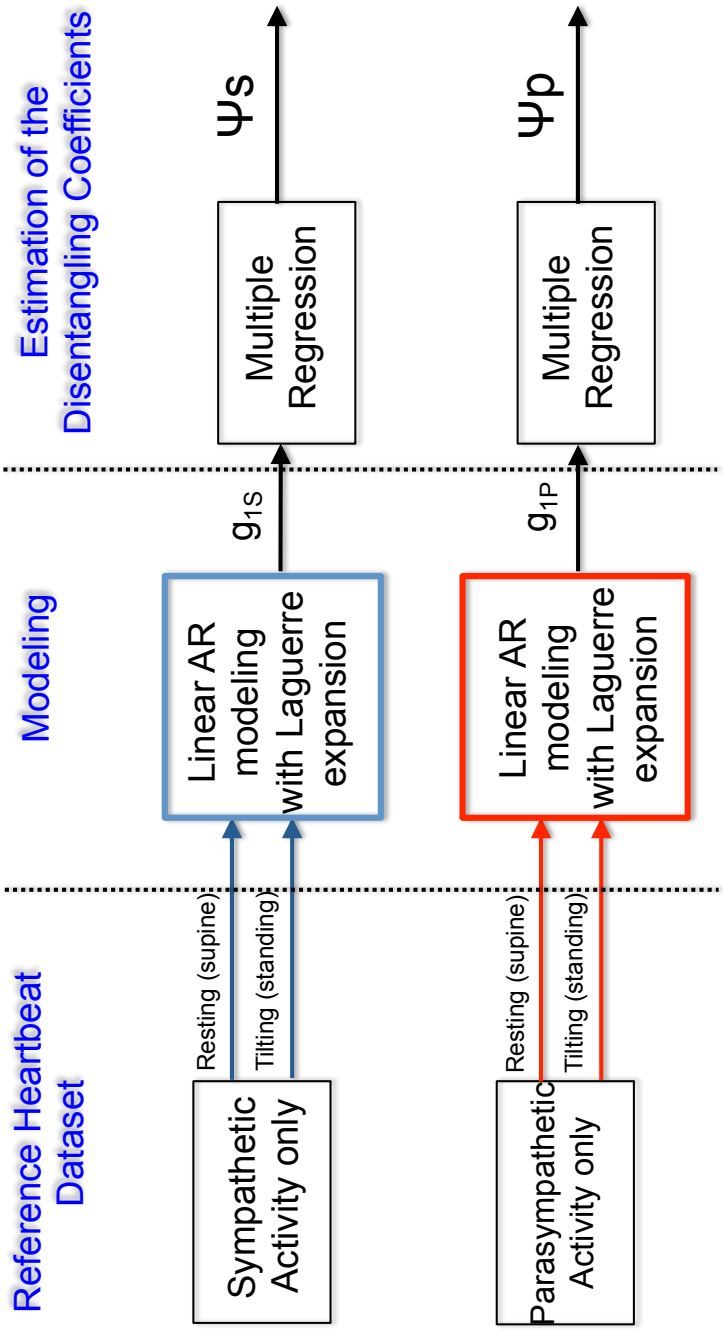

Fig. 11. Scheme detail of the "Model and Multiple Regression" block included in Figure 10.

Experimental results

Goodness of fit analysis: Table VII shows results from a comprehensive goodness of fit analysis performed on the Tilt-table protocol, as well as the Lower Body Negative Pressure and Handgrip protocols. Specifically, we show inter-subject statistics summarized as interval (Median±MAD), minimum and maximum values on the Sum of the Squared Distances of the points outside the confidence interval of the autocorrelation plot, as well as KS distance.

TABLE VII
COMPARISON OF AUTONOMIC INDICES BETWEEN BASELINE AND HANDGRIP

Autonomic Index	**ACP-SSD Squared Distances (SSD) Interval**	**ACP-SSD** Min. (%)	**ACP-SSD** Max. (%)	**KS Distance Interval**	**KS Distance Min.**	**KS Distance Max.**
Tilt-Table	0.024±0.0060	0.0042	0.0459	0.022±0.0056	0.0078	0.0412
Lower Body Negative Pressure	0.0891±0.066	0.001	0.336	0.0366±0.0082	0.0146	0.0797
Handgrip	0.0228±0.0207	0.002	0.160	0.0647±0.0102	0.0373	0.1091

ACP-SSD: Autocorrelation Plot - Sum of the Squared Distances
KS Distance: Kolmogorov-Smirnov Distance
Intervals are expressed as Median±Median absolute deviation

Figure 12 shows exemplary goodness of fit plots (KS and Autocorrelation plots) from data gathered from the Tilt-table and Lower Body Negative Pressure protocols.

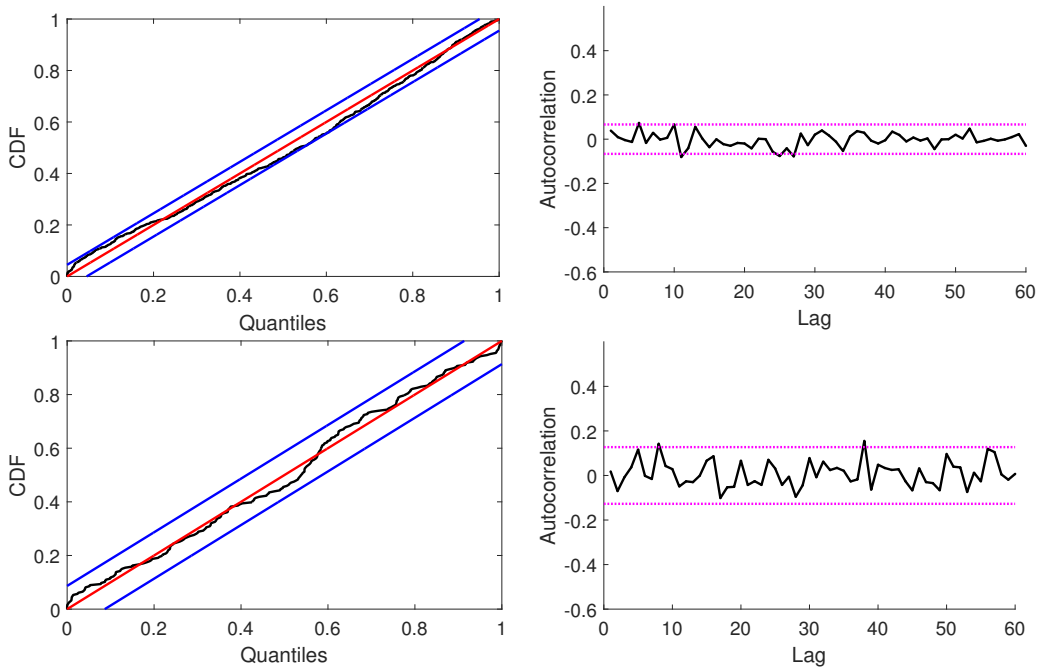

Fig. 12. Exemplary KS (left column) and Autocorrelation (right column) plots from data gathered from the Tilt-table (top row) and Lower Body Negative Pressure (bottom row) protocols. CDF: Cumulative Density Function.

Tilt-table protocol: In order to demonstrate how the proposed SAI and PAI measures are able to follow sympathetic and parasympathetic changes, respectively, at a single-subject level, SAI-PAI estimates along with their LF-HF counterpart, as well as standard instantaneous heartbeat statistics in the time domain are reported here (Median±MAD).

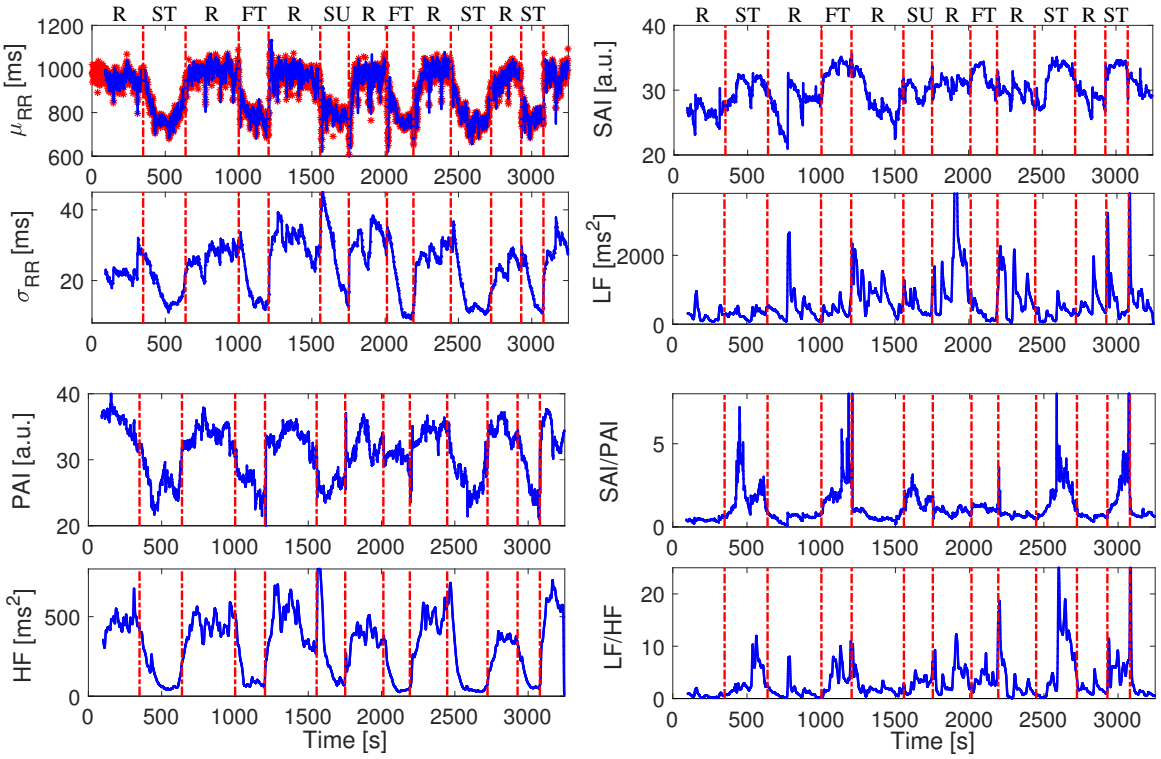

Fig. 13. Instantaneous heartbeat statistics computed from an exemplary subject of the Tilt-Table protocol. In the top-left panel, the estimated $\mu_{RR}(t)$, superimposed on the recorded R-R series, and the instantaneous heartbeat standard deviation $\sigma_{RR}(t)$ are shown. Instantaneous sympathetic and parasympathetic activity, and sympatho-vagal balance as estimated through SAI and PAI, and SAI/PAI ratio measures, along with the LF, HF and LF/HF ratio are shown in the other panels. Vertical dotted red lines indicate the beginning and end of each experimental transition. For this subject, the first transition is from rest (R) to slow tilt (ST) and back, the second is from R to fast tilt (FT) and back, the third and fourth are from R to stand-up (SU) , then R to ST, and the final R to FT and back.. Transitions are randomized for each subject.

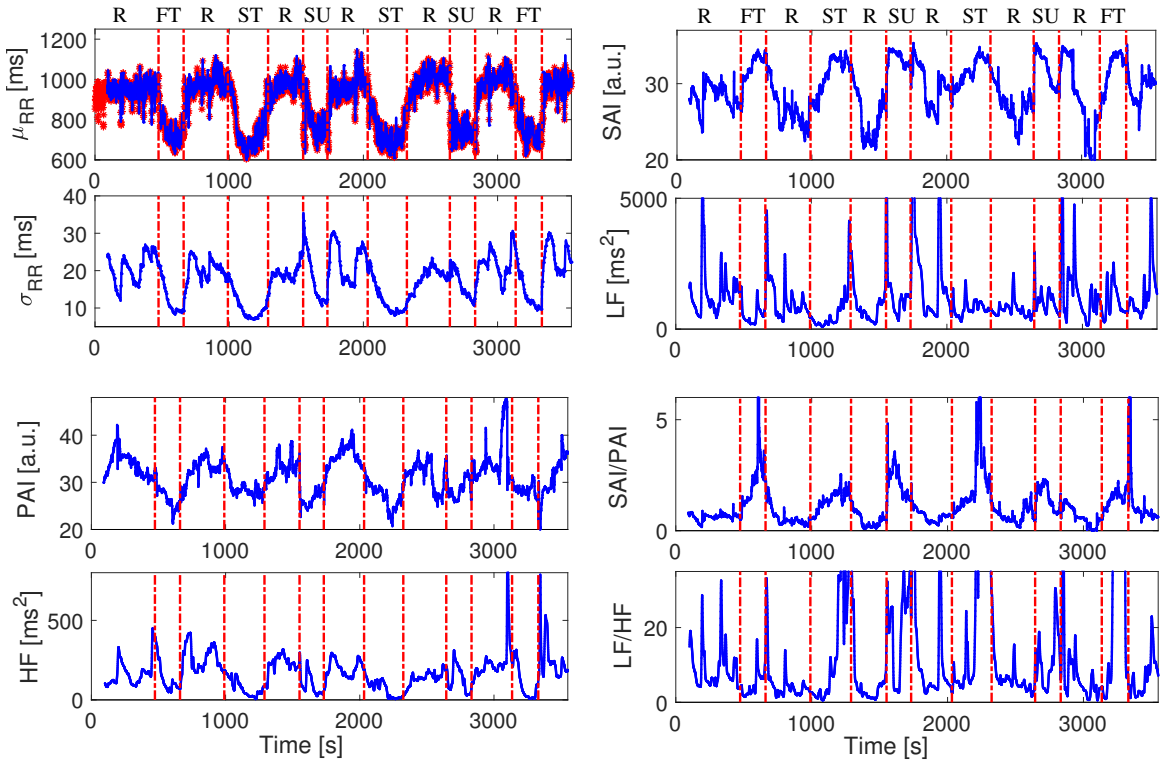

Fig. 14. Instantaneous heartbeat statistics computed from an exemplary subject of the Tilt-Table protocol. In the top-left panel, the estimated $\mu_{RR}(t)$, superimposed on the recorded R-R series, and the instantaneous heartbeat standard deviation $\sigma_{RR}(t)$ are shown. Instantaneous sympathetic and parasympathetic activity, and sympatho-vagal balance as estimated through SAI and PAI, and SAI/PAI ratio measures, along with the LF, HF and LF/HF ratio are shown in the other panels. Vertical dotted red lines indicate the beginning and end of each experimental transition. For this subject, the first transition is from rest (R) to fast tilt (FT) and back, the second is from R to slow tilt (ST) and back, the third is from R to stand-up (SU) , then R to ST, R to SU and R to FT and back.. Transitions are randomized for each subject.

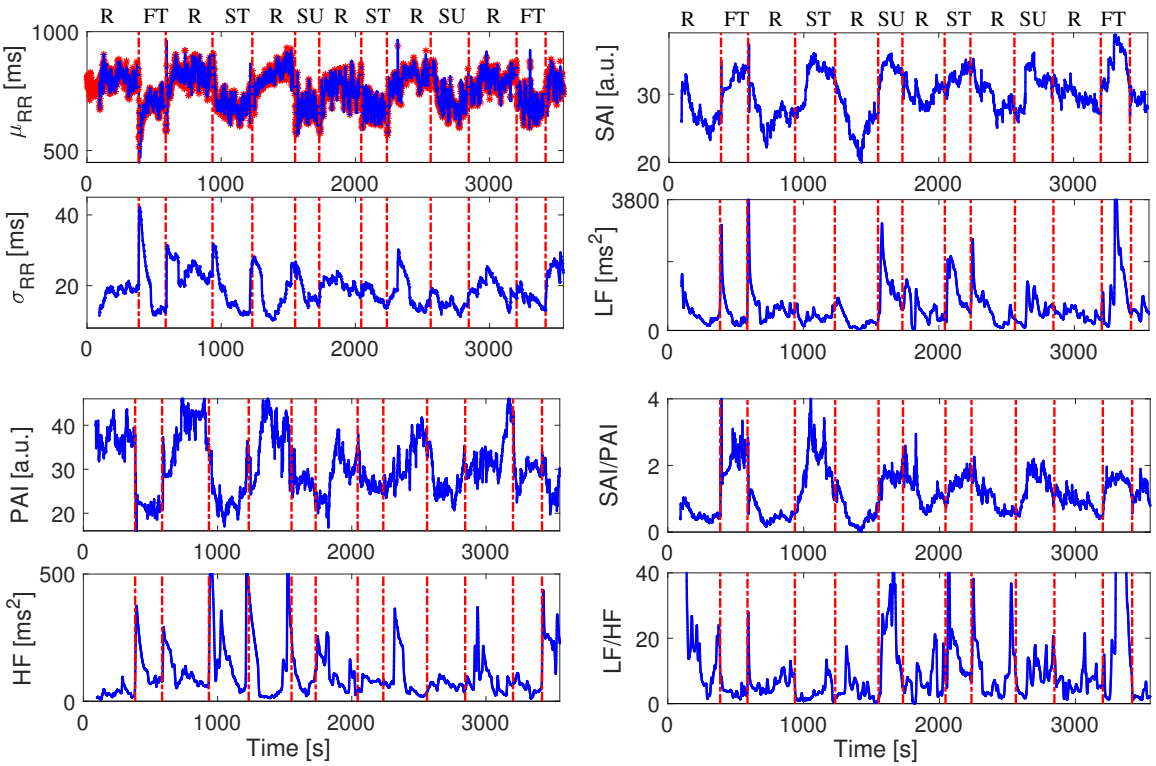

Fig. 15. Instantaneous heartbeat statistics computed from an exemplary subject of the Tilt-Table protocol. In the top-left panel, the estimated $\mu_{RR}(t)$, superimposed on the recorded R-R series, and the instantaneous heartbeat standard deviation $\sigma_{RR}(t)$ are shown. Instantaneous sympathetic and parasympathetic activity, and sympatho-vagal balance as estimated through SAI and PAI, and SAI/PAI ratio measures, along with the LF, HF and LF/HF ratio are shown in the other panels. Vertical dotted red lines indicate the beginning and end of each experimental transition. For this subject, the first transition is from rest (R) to fast tilt (FT) and back, the second is from R to slow tilt (ST) and back, the third and fourth are from R to stand-up (SU) , then R to ST, and the final R to FT and back.. Transitions are randomized for each subject.

Tables VIII, IX, and X show comprehensive results gathered from three estimation methodologies: linear point-process method (AR_{PP}), linear point-process method with Laguerre expansion (ARL_{PP}), and standard linear autoregressive modeling (AR). Through each of these methods, considering rest-to-stand up (Table VIII), rest-to-slow tilt (Table X), and rest-to-fast tilt (Table IX) procedures, the following heartbeat dynamics measures were evaluated: mean RR interval (μ_{RR}), standard deviation of the RR intervals (σ_{RR}), sympathetic and parasympathetic activity, and sympatho-vagal balance.

Table VIII shows similar performances between the three modeling methods while discerning rest from stand up sessions using μ_{RR} and σ_{RR} estimates. The same applies for the estimation of LF, HF, and LF/HF ratio. Nevertheless, the use of ARL_{PP} modeling for the estimation of SAI, PAI, and SAI/PAI measures significantly outperform the use of AR_{PP} and AR modeling for the identification of sympathetic and parasympathetic activities. All SAI and PAI estimates are associated with significant differences between rest and stand up sessions with p-values as low as $< 10^{-5}$.

TABLE VIII
RESULTS FROM THE REST - STAND UP EXPERIMENTAL DATASET

Statistical Index	Model	Rest	Stand-Up	p-value
μ_{RR}(ms)	AR_{PP}	906.17 ± 116.21	774.48 ± 80.41	0.015907
	ARL_{PP}	914.94 ± 122.70	773.46 ± 80.67	0.011924
	AR	910.94 ± 123.08	781.92 ± 55.96	0.013141
σ_{RR}(ms)	AR_{PP}	19.69 ± 9.37	15.84 ± 5.06	0.406973
	ARL_{PP}	19.72 ± 9.37	16.57 ± 4.89	0.521672
	AR	47.48 ± 18.59	48.65 ± 16.42	0.998264
Sympathetic Activity	LF(AR_{PP})	328.54 ± 260.34	410.03 ± 305.24	0.986259
	LF(ARL_{PP})	516.16 ± 311.31	152.33 ± 379.46	0.270000
	LF(AR)	349.86 ± 331.22	514.13 ± 506.35	0.947366
	SAI$_{NEW(0)}$	8.78 ± 1.21	12.55 ± 0.87	0.000078
	SAI$_{NEW(1)}$	8.52 ± 2.08	12.83 ± 0.34	0.000155
	SAI$_{NEW(2)}$	9.14 ± 0.87	10.11 ± 1.17	0.027497
	SAI$_{NEW(3)}$	33.05 ± 5.59	43.56 ± 5.15	0.000256
	SAI$_{NEW(4)}$	30.03 ± 3.17	39.05 ± 2.05	0.000031
Parasympathetic Activity	HF(AR_{PP})	179.39 ± 149.43	76.13 ± 51.63	0.125312
	HF(ARL_{PP})	337.17 ± 247.07	155.23 ± 73.60	0.408000
	HF(AR)	234.17 ± 150.02	121.52 ± 71.68	0.088179
	PAI$_{NEW(0)}$	10.83 ± 1.01	7.16 ± 1.97	0.001805
	PAI$_{NEW(1)}$	11.37 ± 0.84	8.93 ± 1.56	0.028127
	PAI$_{NEW(2)}$	11.42 ± 1.09	10.00 ± 0.38	0.002437
	PAI$_{NEW(3)}$	38.39 ± 3.20	32.03 ± 3.74	0.002631
	PAI$_{NEW(4)}$	35.91 ± 1.84	29.63 ± 3.25	0.000570
Sympatho-Vagal Balance	LF/HF(AR_{PP})	1.37 ± 0.78	2.58 ± 2.41	0.221391
	LF/HF(ARL_{PP})	1.88 ± 1.36	3.25 ± 2.59	0.242000
	LF/HF(AR)	0.87 ± 0.66	0.89 ± 0.89	0.597419
	SAI/PAI$_{NEW(0)}$	0.86 ± 0.30	1.49 ± 0.17	0.002463
	SAI/PAI$_{NEW(1)}$	0.81 ± 0.19	1.35 ± 0.29	0.001088
	SAI/PAI$_{NEW(2)}$	0.80 ± 0.14	1.12 ± 0.11	0.000650
	SAI/PAI$_{NEW(3)}$	0.83 ± 0.18	1.38 ± 0.23	0.000014
	SAI/PAI$_{NEW(4)}$	0.85 ± 0.14	1.29 ± 0.13	0.000003
RMSSD(ms)		26.28 ± 9.78	19.46 ± 4.41	0.144596
pNN50(%)		5.98 ± 5.89	2.18 ± 2.18	0.098656
HRV_tri_ind		8.10 ± 1.71	7.61 ± 2.01	0.605398
TINN (ms)		147.50 ± 40.00	185.00 ± 25.00	0.563922

p-values are obtained from the rank-sum test between the Rest and Stand-up sessions. AR_{PP}: estimates from linear point-process method.
ARL_{PP}: estimates from linear point-process method with Laguerre expansion.
AR: estimates from linear autoregressive model.
NEW(0): a multiple linear regression using subject specific (i.e., performed for each subject) recording from one rest-upright condition.
NEW(1): a multiple linear regression using subject specific (i.e., performed for each subject) recording averaging Ψ_S and Ψ_P estimates from stand-up, slow and fast tilting conditions.
NEW(2): a multiple linear regression using general values (i.e., calculated over all of the subjects), averaging Ψ_S and Ψ_P estimates from stand-up, slow and fast tilting conditions, following a leave one subject out procedure.
NEW(3): a multiple linear regression using general values (i.e., calculated over all of the subjects) averaging Ψ_S and Ψ_P estimates from the rest-tilt control session of an independent dataset.
NEW(4): a multiple linear regression using general values (i.e., calculated over all of the subjects) averaging Ψ_S and Ψ_P from subjects of an independent dataset undergoing autonomic blockade (parasympathetic suppression -> sympathetic kernels Ψ_S; sympathetic suppression -> parasympathetic kernels Ψ_P.

Table IX also shows similar performances between the three modeling methods while discerning rest from slow tilt sessions using μ_{RR}, σ_{RR}, LF, HF, and LF/HF ratio. All SAI and PAI estimates are associated with significant differences between rest and stand up sessions with p-values as low as $< 10^{-3}$.

TABLE IX
RESULTS FROM THE REST - SLOW TILT-TABLE EXPERIMENTAL DATASET

Statistical Index	Model	Rest	Titl-Table Slow	p-value
μ_{RR}(ms)	AR_{PP}	875.25 ± 73.14	765.03 ± 58.91	0.000512
	ARL_{PP}	877.80 ± 72.50	764.79 ± 56.81	0.000412
	AR	879.59 ± 75.09	772.82 ± 46.10	0.001063
σ_{RR}(ms)	AR_{PP}	21.51 ± 6.07	15.13 ± 4.95	0.057883
	ARL_{PP}	22.29 ± 5.92	15.11 ± 4.62	0.057883
	AR	52.57 ± 17.69	62.80 ± 16.30	0.843425
Sympathetic Activity	LF(AR_{PP})	417.76 ± 240.68	332.88 ± 162.72	0.438254
	LF(ARL_{PP})	552.42 ± 388.69	368.13 ± 220.38	0.715000
	LF(AR)	465.03 ± 241.99	394.37 ± 310.24	0.661443
	SAI$_{NEW(0)}$	8.18 ± 1.50	11.14 ± 1.48	0.000965
	SAI$_{NEW(1)}$	9.22 ± 0.80	10.00 ± 1.16	0.052808
	SAI$_{NEW(2)}$	9.26 ± 0.56	10.52 ± 0.72	0.000970
	SAI$_{NEW(3)}$	30.78 ± 5.19	35.54 ± 5.45	0.011087
	SAI$_{NEW(4)}$	33.50 ± 3.17	36.05 ± 1.59	0.007000
Parasympathetic Activity	HF(AR_{PP})	235.59 ± 166.53	88.15 ± 68.42	0.046554
	HF(ARL_{PP})	295.12 ± 192.60	128.92 ± 77.27	0.060000
	HF(AR)	263.67 ± 141.88	150.51 ± 74.30	0.050001
	PAI$_{NEW(0)}$	11.96 ± 2.00	7.27 ± 2.58	0.000177
	PAI$_{NEW(1)}$	14.09 ± 0.41	9.13 ± 2.40	0.001355
	PAI$_{NEW(2)}$	11.66 ± 0.93	10.25 ± 0.65	0.000708
	PAI$_{NEW(3)}$	39.14 ± 2.67	36.02 ± 1.01	0.066003
	PAI$_{NEW(4)}$	36.42 ± 2.92	31.96 ± 3.15	0.011000
Sympatho-Vagal Balance	LF/HF(AR_{PP})	1.03 ± 0.74	2.73 ± 1.64	0.209343
	LF/HF(ARL_{PP})	1.39 ± 1.071	3.00 ± 1.43	0.126000
	LF/HF(AR)	0.66 ± 0.23	1.21 ± 0.68	0.168735
	SAI/PAI$_{NEW(0)}$	0.66 ± 0.19	1.51 ± 0.69	0.000189
	SAI/PAI$_{NEW(1)}$	0.63 ± 0.09	1.18 ± 0.33	0.000376
	SAI/PAI$_{NEW(2)}$	0.82 ± 0.12	0.95 ± 0.07	0.004746
	SAI/PAI$_{NEW(3)}$	0.81 ± 0.20	1.05 ± 0.21	0.007233
	SAI/PAI$_{NEW(4)}$	0.95 ± 0.13	1.15 ± 0.13	0.001000
RMSSD(ms)		32.10 ± 12.56	19.68 ± 4.52	<0.05
pNN50(%)		10.20 ± 9.47	1.74 ± 1.37	<0.02
HRV_tri_ind		8.03 ± 1.41	7.31 ± 1.61	>0.05
TINN (ms)		195.00 ± 70.00	150.00 ± 45.00	>0.05

p-values are obtained from the rank-sum test between the Rest and Slow-Tilt sessions. AR_{PP}: estimates from linear point-process method.
ARL_{PP}: estimates from linear point-process method with Laguerre expansion.
AR: estimates from linear autoregressive model.
NEW(0): a multiple linear regression using subject specific (i.e., performed for each subject) recording from one rest-upright condition.
NEW(1): a multiple linear regression using subject specific (i.e., performed for each subject) recording averaging Ψ_S and Ψ_P estimates from stand-up, slow and fast tilting conditions.
NEW(2): a multiple linear regression using general values (i.e., calculated over all of the subjects), averaging Ψ_S and Ψ_P estimates from stand-up, slow and fast tilting conditions, following a leave one subject out procedure.
NEW(3): a multiple linear regression using general values (i.e., calculated over all of the subjects) averaging Ψ_S and Ψ_P estimates from the rest-tilt control session of an independent dataset.
NEW(4): a multiple linear regression using general values (i.e., calculated over all of the subjects) averaging Ψ_S and Ψ_P from subjects of an independent dataset undergoing autonomic blockade (parasympathetic suppression -> sympathetic kernels Ψ_S; sympathetic suppression -> parasympathetic kernels Ψ_P.

Table X also shows similar performances between the three modeling methods while discerning rest from fast tilt sessions using μ_{RR}, σ_{RR}, LF, HF, and LF/HF ratio. All SAI and PAI estimates are associated with significant differences between rest and stand up sessions with p-values as low as $< 10^{-3}$.

TABLE X
RESULTS FROM THE REST - FAST TILT-TABLE EXPERIMENTAL DATASET

Statistical Index	Model	Rest	Titl-Table Fast	p-value
μ_{RR}(ms)	AR_{PP}	881.03 ± 94.55	776.18 ± 66.49	0.004627
	ARL_{PP}	883.03 ± 95.78	774.62 ± 54.46	0.005068
	AR	860.50 ± 80.48	777.18 ± 51.58	0.009375
σ_{RR}(ms)	AR_{PP}	21.68 ± 8.02	16.33 ± 4.00	0.064190
	ARL_{PP}	22.18 ± 8.31	16.92 ± 4.51	0.073844
	AR	48.20 ± 9.40	46.00 ± 15.01	0.318951
Sympathetic Activity	LF(AR_{PP})	476.41 ± 285.63	349.72 ± 203.75	0.303830
	LF(ARL_{PP})	568.28 ± 299.64	504.37 ± 269.77	0.704000
	LF(AR)	401.86 ± 330.31	338.33 ± 278.42	0.739734
	$\text{SAI}_{NEW(0)}$	10.14 ± 1.30	12.21 ± 1.43	0.002616
	$\text{SAI}_{NEW(1)}$	9.51 ± 0.50	12.95 ± 2.07	0.013986
	$\text{SAI}_{NEW(2)}$	9.33 ± 0.50	10.70 ± 0.49	0.000156
	$\text{SAI}_{NEW(3)}$	33.70 ± 5.42	41.42 ± 3.33	0.002173
	$\text{SAI}_{NEW(4)}$	31.80 ± 2.21	36.79 ± 1.85	0.000870
Parasympathetic Activity	HF(AR_{PP})	214.90 ± 159.75	123.14 ± 79.59	0.103231
	HF(ARL_{PP})	239.12 ± 177.12	203.04 ± 102.98	0.815000
	HF(AR)	296.05 ± 153.27	136.80 ± 59.81	0.023688
	$\text{PAI}_{NEW(0)}$	10.77 ± 0.81	8.17 ± 1.90	0.001019
	$\text{PAI}_{NEW(1)}$	11.59 ± 0.91	8.56 ± 1.48	0.002331
	$\text{PAI}_{NEW(2)}$	11.69 ± 1.39	10.46 ± 0.67	0.027591
	$\text{PAI}_{NEW(3)}$	39.13 ± 3.15	34.12 ± 1.84	0.002259
	$\text{PAI}_{NEW(4)}$	35.89 ± 2.95	30.62 ± 1.58	0.002000
Sympatho-Vagal Balance	LF/HF(AR_{PP})	2.05 ± 1.57	1.96 ± 1.26	0.753865
	LF/HF(ARL_{PP})	1.82 ± 1.43	1.56 ± 0.65	0.977000
	LF/HF(AR)	0.93 ± 0.46	1.51 ± 1.10	0.116943
	$\text{SAI/PAI}_{NEW(0)}$	0.83 ± 0.35	1.74 ± 0.47	0.000612
	$\text{SAI/PAI}_{NEW(1)}$	0.85 ± 0.18	1.57 ± 0.31	0.011072
	$\text{SAI/PAI}_{NEW(2)}$	0.84 ± 0.16	1.03 ± 0.07	0.000977
	$\text{SAI/PAI}_{NEW(3)}$	0.94 ± 0.22	1.25 ± 0.13	0.000704
	$\text{SAI/PAI}_{NEW(4)}$	0.87 ± 0.13	1.21 ± 0.13	0.000263
RMSSD(ms)		28.70 ± 11.32	18.10 ± 3.60	0.038235
pNN50(%)		6.54 ± 6.18	1.14 ± 1.14	0.018120
HRV_tri_ind		8.49 ± 2.00	6.50 ± 0.93	0.062213
TINN (ms)		182.50 ± 60.00	140.00 ± 45.00	0.160440

p-values are obtained from the rank-sum test between the Rest and Fast-Tilt sessions. AR_{PP}: estimates from linear point-process method.
ARL_{PP}: estimates from linear point-process method with Laguerre expansion.
AR: estimates from linear autoregressive model.
NEW(0): a multiple linear regression using subject specific (i.e., performed for each subject) recording from one rest-upright condition.
NEW(1): a multiple linear regression using subject specific (i.e., performed for each subject) recording averaging Ψ_S and Ψ_P estimates from stand-up, slow and fast tilting conditions.
NEW(2): a multiple linear regression using general values (i.e., calculated over all of the subjects), averaging Ψ_S and Ψ_P estimates from stand-up, slow and fast tilting conditions, following a leave one subject out procedure.
NEW(3): a multiple linear regression using general values (i.e., calculated over all of the subjects) averaging Ψ_S and Ψ_P estimates from the rest-tilt control session of an independent dataset.
NEW(4): a multiple linear regression using general values (i.e., calculated over all of the subjects) averaging Ψ_S and Ψ_P from subjects of an independent dataset undergoing autonomic blockade (parasympathetic suppression -> sympathetic kernels Ψ_S; sympathetic suppression -> parasympathetic kernels Ψ_P.

Autonomic Blockade: For the sake of completeness, we here report results and related statistics (Median±MAD) considering postural changes during control and sympathetic/parasympathetic blockades, following a previously validated approach described in [41].

During the control postural changes, SAI and PAI estimates, along with their ratio, follow physiologically plausible trends (i.e., SAI increases after standing with respect to rest; PAI decreases after standing with respect to rest). As expected, autonomic blockades make SAI and PAI reaching relative minimum and maximal values. Specifically, the PAI is at a minimum in the upright+atropine case (i.e., parasympathetic blockade after standing) and at maximum in the supine+propanolol case (i.e., resting state during sympathetic blockade), whereas the SAI is at a maximum in the control standing case, and at a minimum in the supine+propranolol case (i.e., resting state during sympathetic blockade). Consistently, the sympathovagal balance SAI/PAI is at minimum in the supine+propanolol case (i.e., resting state during sympathetic blockade), and at maximum in the upright+atropine case (i.e., parasympathetic blockade after standing).

TABLE XI

Autonomic Index	**Control Test (14 Subjects)** No Drugs			**Control and Autonomic Blockade (7+7 Subjects)** Control/Propranorol	Control/Athropine
	Rest	**Standing**	**p-val**	**Rest**	**Standing**
SAI [a.u.]	40.010 ± 2.046	42.569 ± 1.339	0.001	34.921 ± 1.086	43.668 ± 2.342
PAI [a.u.]	30.308 ± 1.243	28.544 ± 1.218	0.048	30.825 ± 1.08	23.469 ±4.689
SAI/PAI	1.357 ± 0.156	1.514 ± 0.079	0.024	1.129 ± 0.099	1.667 ± 0.229

p-values are from the signrank non-parametric test for paired data

REFERENCES

[1] **Akselrod S**, "Components of heart rate variability: basic studies," *Heart rate variability*, pp. 147–163, 1995.

[2] **Akselrod S, Gordon D, Madwed J, Snidman N, Shannon D, Cohen R**, "Hemodynamic regulation: investigation by spectral analysis," *American Journal of Physiology-Heart and Circulatory Physiology*, vol. 249, no. 4, p. H867, 1985.

[3] **Akselrod S, Gordon D, Ubel F, Shannon D, Berger A, Cohen R**, "Power spectrum analysis of heart rate fluctuation: a quantitative probe of beat-to-beat cardiovascular control," *Science*, vol. 213, no. 4504, p. 220, 1981.

[4] **Andersen P**, *Statistical models based on counting processes*. Springer Verlag, 1993.

[5] **Armoundas AA, Chon KH**, "Method and apparatus for detection and treatment of autonomic system imbalance," Jul. 6 2007, uS Patent App. 12/373,227.

[6] **Barbieri R, Brown EN**, "Analysis of heartbeat dynamics by point process adaptive filtering," *Biomedical Engineering, IEEE Transactions on*, vol. 53, no. 1, pp. 4–12, 2006.

[7] **Barbieri R, Matten E, Alabi A, Brown EN**, "A point-process model of human heartbeat intervals: new definitions of heart rate and heart rate variability," *American Journal of Physiology-Heart and Circulatory Physiology*, vol. 288, no. 1, p. H424, 2005.

[8] **Batzel J, Baselli G, Mukkamala R, Chon KH**, "Modelling and disentangling physiological mechanisms: linear and nonlinear identification techniques for analysis of cardiovascular regulation," *Philosophical Transactions of the Royal Society of London A: Mathematical, Physical and Engineering Sciences*, vol. 367, no. 1892, pp. 1377–1391, 2009.

[9] **Berger R, Saul J, Cohen R**, "Transfer function analysis of autonomic regulation. I. Canine atrial rate response," *American Journal of Physiology-Heart and Circulatory Physiology*, vol. 256, no. 1, p. H142, 1989.

[10] **Chen X, Mukkamala R**, "Selective quantification of the cardiac sympathetic and parasympathetic nervous systems by multisignal analysis of cardiorespiratory variability," *American Journal of Physiology-Heart and Circulatory Physiology*, vol. 294, no. 1, p. H362, 2008.

[11] **Chen Z, Brown EN, Barbieri R**, "Assessment of autonomic control and respiratory sinus arrhythmia using point process models of human heart beat dynamics," *Biomedical Engineering, IEEE Transactions on*, vol. 56, no. 7, pp. 1791–1802, 2009.

[12] **Chen Z, Purdon P, Harrell G, Pierce E, Walsh J, Brown EN, Barbieri R**, "Dynamic assessment of baroreflex control of heart rate during induction of propofol anesthesia using a point process method," *Annals of biomedical engineering*, pp. 1–17, 2011.

[13] **Chon KH, Yang B, Siu KL, Rolle M, Obrosova IG, Brink PR, Birzgalis A, Moore LC**, "A novel quantitative method for diabetic cardiac autonomic neuropathy assessment in type I diabetic mice," *American Journal of Physiology-Heart and Circulatory Physiology*, 2013.

[14] **Citi L, Brown EN, Barbieri R**, "A real-time automated point-process method for the detection and correction of erroneous and ectopic heartbeats," *IEEE transactions on biomedical engineering*, vol. 59, no. 10, pp. 2828–2837, 2012.

[15] **Esler M, Rumantir M, Wiesner G, Kaye D, Hastings J, Lambert G**, "Sympathetic nervous system and insulin resistance: from obesity to diabetes," *American journal of hypertension*, vol. 14, no. S7, pp. 304S–309S, 2001.

[16] **Floras JS, Legault L, Morali GA, Hara K, Blendis LM**, "Increased sympathetic outflow in cirrhosis and ascites: direct evidence from intraneural recordings," *Annals of internal medicine*, vol. 114, no. 5, pp. 373–380, 1991.

[17] **Goldstein DS, Bentho O, Park MY, Sharabi Y**, "Low-frequency power of heart rate variability is not a measure of cardiac sympathetic tone but may be a measure of modulation of cardiac autonomic outflows by baroreflexes," *Experimental physiology*, vol. 96, no. 12, pp. 1255–1261, 2011.

[18] **Grassi G**, "Role of the sympathetic nervous system in human hypertension," *Journal of hypertension*, vol. 16, no. 12, pp. 1979–1987, 1998.

[19] **Grassi G, Esler M**, "How to assess sympathetic activity in humans," *Journal of hypertension*, vol. 17, no. 6, pp. 719–734, 1999.

[20] **Heldt T, Oefinger MB, Hoshiyama M, Mark RG**, "Circulatory response to passive and active changes in posture," *Computers in Cardiology*, vol. 30, pp. 263–266, 2003.

[21] **Heldt T, Shim EB, Kamm RB, Mark RG**, "Computational modeling of cardiovascular response to orthostatic stress," *Journal of Applied Physiology (Bethesda, Md.: 1985)*, vol. 92, no. 3, pp. 1239–1254, Mar. 2002.

[22] **Hirsch J, Bishop B**, "Respiratory sinus arrhythmia in humans: how breathing pattern modulates heart rate," *American Journal of Physiology-Heart and Circulatory Physiology*, vol. 241, no. 4, p. H620, 1981.

[23] **Houle M, Billman G**, "Low-frequency component of the heart rate variability spectrum: a poor marker of sympathetic activity," *American Journal of Physiology-Heart and Circulatory Physiology*, vol. 276, no. 1, p. H215, 1999.

[24] **Kamath M, Fallen E**, "Power spectral analysis of heart rate variability: a noninvasive signature of cardiac autonomic function." *Critical reviews in biomedical engineering*, vol. 21, no. 3, p. 245, 1993.

[25] **Kaye DM, Lambert GW, Lefkovits J, Morris M, Jennings G, Esler MD**, "Neurochemical evidence of cardiac sympathetic activation and increased central nervous system norepinephrine turnover in severe congestive heart failure," *Journal of the American College of Cardiology*, vol. 23, no. 3, pp. 570–578, 1994.

[26] **Koepchen H**, "History of studies and concepts of blood pressure waves," *Mechanisms of blood pressure waves*, pp. 3–23, 1984.

[27] **Levy M**, "Sympathetic–parasympathetic interactions in heart," *Circ. Res.*, vol. 29, no. 437, 1972.

[28] **Malliani A**, "Association of heart rate variability components with physiological regulatory mechanisms," *Heart rate variability*, pp. 173–188, 1995.

[29] **Malliani A, Julien C, Billman G, Cerutti S, Piepoli M, Bernardi L, Sleight P, Cohen M, Tan C, Laude D, Elstad M, Toska K, Evans J, Eckberg D**, "Cardiovascular variability is/is not an index of autonomic control of circulation," *Journal of Applied Physiology*, vol. 101, pp. 684–688, 2006.

[30] **Malpas S**, "Neural influences on cardiovascular variability: possibilities and pitfalls," *American Journal of Physiology-Heart and Circulatory Physiology*, vol. 282, no. 1, p. H6, 2002.

[31] **Mancia G, Grassi G**, "The autonomic nervous system and hypertension," *Circulation research*, vol. 114, no. 11, pp. 1804–1814, 2014.

[32] **Marmarelis V**, "Identification of nonlinear biological system using Laguerre expansions of kernels," *Ann. Biomed. Eng.*, vol. 21, pp. 573–589, 1993.

[33] **McCrory C, Berkman LF, Nolan H, OÕLeary N, Foley M, Kenny RA**, "Speed of heart rate recovery in response to orthostatic challengenovelty and significance," *Circulation research*, vol. 119, no. 5, pp. 666–675, 2016.

[34] **Mitsis G, Zhang R, Levine B, Marmarelis V**, "Modeling of nonlinear physiological systems with fast and slow dynamics. ii. application to cerebral autoregulation," *Annals of biomedical engineering*, vol. 30, no. 4, pp. 555–565, 2002.

[35] **Parati G, Esler M**, "The human sympathetic nervous system: its relevance in hypertension and heart failure," *European heart journal*, p. ehs041, 2012.

[36] **Pomeranz B, Macaulay R, Caudill M, Kutz I, Adam D, Gordon D, Kilborn K, Barger A, Shannon D, Cohen R *et al.***, "Assessment of autonomic function in humans by heart rate spectral analysis," *American Journal of Physiology-Heart and Circulatory Physiology*, vol. 248, no. 1, p. H151, 1985.

[37] **Posada-Quintero HF, Florian JP, Orjuela-Cañón AD, Aljama-Corrales T, Charleston-Villalobos S, Chon KH**, "Power spectral density analysis of electrodermal activity for sympathetic function assessment," *Annals of biomedical engineering*, pp. 1–12, 2016.

[38] **Rajendra Acharya U, Paul Joseph K, Kannathal N, Lim C, Suri J**, "Heart rate variability: a review," *Medical and Biological Engineering and Computing*, vol. 44, no. 12, pp. 1031–1051, 2006.

[39] **Reyes del Paso GA, Langewitz W, Mulder LJ, Roon A, Duschek S**, "The utility of low frequency heart rate variability as an index of sympathetic cardiac tone: a review with emphasis on a reanalysis of previous studies," *Psychophysiology*, vol. 50, no. 5, pp. 477–487, 2013.

[40] **Sassi R, Cerutti S, Lombardi F, Malik M, Huikuri HV, Peng CK, Schmidt G, Yamamoto Y, Gorenek B, Lip GH *et al.***, "Advances in heart rate variability signal analysis: joint position statement by the e-cardiology ESC working group and the European heart rhythm association co-endorsed by the Asia Pacific heart rhythm society," *Europace*, p. euv015, 2015.

[41] **Saul J, Berger R, Albrecht P, Stein S, Chen M, Cohen R**, "Transfer function analysis of the circulation: unique insights into cardiovascular regulation," *American Journal of Physiology-Heart and Circulatory Physiology*, vol. 261, no. 4, p. H1231, 1991.

[42] **Schetzen M**, "The volterra and wiener theories of nonlinear systems," 1980.

[43] **Schwartz P, De Ferrari G**, "Sympathetic–parasympathetic interaction in health and disease: abnormalities and relevance in heart failure," *Heart failure reviews*, pp. 1–7, 2010.
[44] **Sinski M, Lewandowski J, Abramczyk P, Narkiewicz K, Gaciong Z**, "Why study sympathetic nervous system," *J Physiol Pharmacol*, vol. 57, no. Suppl 11, pp. 79–92, 2006.
[45] **Sunagawa K, Kawada T, Nakahara T**, "Dynamic nonlinear vago-sympathetic interaction in regulating heart rate," *Heart and Vessels*, vol. 13, no. 4, pp. 157–174, 1998.
[46] **Tahsili-Fahadan P, Geocadin RG**, "Heart–brain axis," *Circulation research*, vol. 120, no. 3, pp. 559–572, 2017.
[47] **Task Force of the European Society of Cardiology, the North American Society of Pacing, and Electrophysiology**, "Heart rate variability: standards of measurement, physiological interpretation and clinical use." *Circulation*, vol. 93, no. 5, pp. 1043–65, 1996.
[48] **Taylor J, Carr D, Myers C, Eckberg D**, "Mechanisms underlying very-low-frequency RR-interval oscillations in humans," *Circulation*, vol. 98, no. 6, pp. 547–555, 1998.
[49] **Treskes R, Velde E, Barendse R, Bruining N**, "Mobile health in cardiology: a review of currently available medical apps and equipment for remote monitoring," *Expert Review of Medical Devices*, no. just-accepted, 2016.
[50] **Ursino M, Magosso E**, "Role of short-term cardiovascular regulation in heart period variability: a modeling study," *American Journal of Physiology-Heart and Circulatory Physiology*, vol. 284, no. 4, p. H1479, 2003.
[51] **Valenza G, Citi L, Barbieri R**, "Estimation of instantaneous complex dynamics through lyapunov exponents: a study on heartbeat dynamics," *PloS one*, vol. 9, no. 8, p. e105622, 2014.
[52] **Valenza G, Citi L, Lanata A, Scilingo EP, Barbieri R**, "Revealing real-time emotional responses: a personalized assessment based on heartbeat dynamics," *Scientific reports*, vol. 4, 2014.
[53] **Valenza G, Citi L, Scilingo EP, Barbieri R**, "Point-process nonlinear models with Laguerre and Volterra expansions: Instantaneous assessment of heartbeat dynamics," *IEEE Transactions on Signal Processing*, vol. 61, no. 11, pp. 2914–2926, 2013.
[54] **Valenza G, Citi L, Scilingo EP, Barbieri R**, "Inhomogeneous point-process entropy: An instantaneous measure of complexity in discrete systems," *Physical Review E*, vol. 89, no. 5, p. 052803, 2014.
[55] **Valenza G, Orsolini S, Diciotti S, Citi L, Scilingo EP, Guerrisi M, Danti S, Lucetti C, Tessa C, Barbieri R *et al.***, "Assessment of spontaneous cardiovascular oscillations in parkinson's disease," *Biomedical Signal Processing and Control*, vol. 26, pp. 80–89, 2016.
[56] **Vaz M, Jennings G, Turner A, Cox H, Lambert G, Esler M**, "Regional sympathetic nervous activity and oxygen consumption in obese normotensive human subjects," *Circulation*, vol. 96, no. 10, pp. 3423–3429, 1997.
[57] **Veith RC, Lewis N, Linares OA, Barnes RF, Raskind MA, Villacres EC *et al.***, "Sympathetic nervous system activity in major depression: basal and desipramine-induced alterations in plasma norepinephrine kinetics," *Archives of general psychiatry*, vol. 51, no. 5, pp. 411–422, 1994.
[58] **Vetter R, Vesin J, Celka P, Scherrer U**, "Observer of the human cardiac sympathetic nerve activity using noncausal blind source separation," *Biomedical Engineering, IEEE Transactions on*, vol. 46, no. 3, pp. 322–330, 1999.
[59] **Vetter R, Virag N, Vesin J, Celka P, Scherrer U**, "Observer of autonomic cardiac outflow based on blind source separation of ECG parameters," *Biomedical Engineering, IEEE Transactions on*, vol. 47, no. 5, pp. 578–582, 2000.
[60] **Wac K**, "Smartphone as a personal, pervasive health informatics services platform: literature review." *Yearbook of medical informatics*, vol. 7, p. 83, 2012.
[61] **Wyller VB, Barbieri R, Saul JP**, "Blood pressure variability and closed-loop baroreflex assessment in adolescent chronic fatigue syndrome during supine rest and orthostatic stress," *European journal of applied physiology*, vol. 111, no. 3, pp. 497–507, 2011.
[62] **Wyller VB, Saul JP, Barbieri R, de Lange C, Hopp E, Norum IB, Thaulow E**, "Autonomic heart rate control at rest and during unloading of the right ventricle in repaired tetralogy of fallot in adolescents," *The American journal of cardiology*, vol. 102, no. 8, pp. 1085–1089, 2008.
[63] **Xiao X, Mukkamala R, Cohen R**, "A selective quantification of cardiac sympathetic and parasympathetic control and its validation through pharmacological blockade," in *Computers in Cardiology, 2004*. IEEE, 2004, pp. 477–480.
[64] **Xiao X, Mukkamala R, Sheynberg N, Grenon SM, Ehrman MD, Mullen TJ, Ramsdell CD, Williams GH, Cohen RJ**, "Effects of simulated microgravity on closed-loop cardiovascular regulation and orthostatic intolerance: analysis by means of system identification," *Journal of Applied Physiology*, vol. 96, no. 2, pp. 489–497, 2004.
[65] **Yasuma F, Hayano J**, "Respiratory sinus arrhythmia*," *Chest*, vol. 125, no. 2, pp. 683–690, 2004.
[66] **Zhong Y, Jan K, Ju K, Chon K**, "Quantifying cardiac sympathetic and parasympathetic nervous activities using principal dynamic modes analysis of heart rate variability," *American Journal of Physiology-Heart and Circulatory Physiology*, vol. 291, no. 3, p. H1475, 2006.
[67] **Zhong Y, Wang H, Ju KH, Jan KM, Chon KH**, "Nonlinear analysis of the separate contributions of autonomic nervous systems to heart rate variability using principal dynamic modes," *IEEE transactions on biomedical engineering*, vol. 51, no. 2, pp. 255–262, 2004.
[68] **Zong W, Moody G**, "WQRS-single-channel QRS detector based on length transform," *Physionet. http://www.physionet.org/physiotools/wag/wqrs-1.htm*, 2003.

IX. Figure Legend

Figure 1: Laguerre polynomials of order 8 for $\alpha = 0.2$ plotted over the first 40 lags

Figure 2: Instantaneous heartbeat statistics computed from an exemplary subject of the Tilt-Table protocol. In the top-left panel, the estimated $\mu_{RR}(t)$, superimposed on the recorded R-R series, and the instantaneous heartbeat standard deviation $\sigma_{RR}(t)$ are shown. Instantaneous sympathetic and parasympathetic activity, and sympatho-vagal balance as estimated through SAI and PAI, and SAI/PAI ratio measures, along with the LF, HF and LF/HF ratio are shown in the other panels. Vertical dotted red lines indicate the beginning and end of each experimental transition. For this subject, the first transition is from rest (R) to stand-up (SU) and back, the second is from R to fast tilt (FT) and back, the third from R to SU, then R to FT, and the final two are from R to slow tilt (ST) and back.. Transitions are randomized for each subject.

Figure 3: TILT-TABLE PROTOCOL: FAST-TILT. Instantaneous point-process estimates averaged along all subjects, aligned with the transitions before and after fast-tilt. In the left panels the estimated instantaneous power $LF(t)$ and the SAI(t) can be compared. At each time, the median value is superimposed (black line) on the standard error of the median (gray area). Vertical red line indicates the beginning of the fast-tilt maneuver. Likewise, the estimated instantaneous power $HF(t)$ and the PAI(t) are shown in the central panels, whereas the estimated instantaneous $LF/HF(t)$ and the SAI/PAI(t) can be compared in the right panels.

Figure 4: TILT-TABLE PROTOCOL: SLOW-TILT. Instantaneous point-process estimates averaged along all subjects, aligned with the slow-tilt transitions. In the left panel, the estimated instantaneous power $LF(t)$ and the SAI(t) can be compared. At each time, the median value is superimposed (black line) on the standard error of the median (gray area). The two vertical red lines indicate the start and end of the slow tilting manoeuver. Likewise, the estimated instantaneous power $HF(t)$ and the PAI(t) can be compared in the central panels, whereas the estimated instantaneous $LF/HF(t)$ and the SAI/PAI(t) can be compared in the right panels.

Figure 5: TILT-TABLE PROTOCOL: STAND UP. Instantaneous point-process estimates averaged along all subjects, aligned with the stand-up transitions. In the left panels, the estimated instantaneous power $LF(t)$ and the SAI(t) can be compared. At each time, the median value is superimposed (black line) on the standard error of the median (gray area). Vertical red lines indicate the beginning of the stand-up maneuver. Likewise, the estimated instantaneous power $HF(t)$ and the PAI(t) can be compared in the central panels, whereas the estimated instantaneous $LF/HF(t)$ and the SAI/PAI(t) can be compared in the right panels.

Figure 6: LBNP PROTOCOL. Instantaneous point-process estimates averaged along all subjects, aligned with the LBNP transitions. In the left panel the estimated instantaneous power $LF(t)$ and the SAI(t) are shown. At each time, the median value is superimposed (black line) on the standard error of the median (gray area). Vertical red line indicates the beginning of the LBNP maneuver. Likewise, the estimated instantaneous power $HF(t)$ and the PAI(t) are shown in the central panel, whereas the estimated instantaneous $LF/HF(t)$ and the SAI/PAI(t) are shown in the right panel.

Figure 7: HANDGRIP PROTOCOL. Instantaneous point-process estimates averaged along all subjects, aligned with the handgrip transitions. In the left panel the estimated instantaneous power $LF(t)$ and the SAI(t) are shown. At each time, the median value is superimposed (black line) on the standard error of the median (gray area). Vertical red line indicates the beginning of the handgrip task. Likewise, the estimated instantaneous power $HF(t)$ and the PAI(t) are shown in the central panel, whereas the estimated instantaneous $LF/HF(t)$ and the SAI/PAI(t) are shown in the right panel.

Figure 8: (Left) First 4 Laguerre Functions for $\alpha = 0.2$ plotted over the first 25 lags. The order of each Laguerre basis is indicated under brackets. (Right) The 3^{rd} Laguerre functions for $\alpha = 0.1, 0.2, 0.3, 0.4$. The corresponding α value is indicated under brackets.

Figure 9: A graphical representation of point-process modeling of heartbeat dynamics. The horizontal axis represents the counting process along the number of heartbeats, whereas the vertical axis represents the duration of heartbeat intervals. Inverse-Gaussian (IG) distributions (green lines on the right) characterize the prediction of the future heartbeat event along the time (from [55])

Figure 10: Block scheme of the modeling and estimation stages involved in the SAI-PAI calculation.

Figure 11: Scheme detail of the "Model and Multiple Regression" block included in Figure 10.

Figure 12: Exemplary KS (left column) and Autocorrelation (right column) plots from data gathered from the Tilt-table (top row) and Lower Body Negative Pressure (bottom row) protocols. CDF: Cumulative Density Function.

Figure 13: Instantaneous heartbeat statistics computed from an exemplary subject of the Tilt-Table protocol. In the top-left panel, the estimated $\mu_{RR}(t)$, superimposed on the recorded R-R series, and the instantaneous heartbeat standard deviation $\sigma_{RR}(t)$ are shown. Instantaneous sympathetic and parasympathetic activity, and sympatho-vagal balance as estimated through SAI and PAI, and SAI/PAI ratio measures, along with the LF, HF and LF/HF ratio are shown in the other panels. Vertical dotted red lines indicate the beginning and end of each experimental transition. For this subject, the first transition is from rest (R) to slow tilt (ST) and back, the second is from R to fast tilt (FT) and back, the third and fourth are from R to stand-up (SU) , then R to ST, and the final R to FT and back.. Transitions are randomized for each subject.

Figure 14: Instantaneous heartbeat statistics computed from an exemplary subject of the Tilt-Table protocol. In the top-left panel, the estimated $\mu_{RR}(t)$, superimposed on the recorded R-R series, and the instantaneous heartbeat standard deviation $\sigma_{RR}(t)$ are shown. Instantaneous sympathetic and parasympathetic activity, and sympatho-vagal balance as estimated through SAI and PAI, and SAI/PAI ratio measures, along with the LF, HF and LF/HF ratio are shown in the other panels. Vertical dotted red lines indicate the beginning and end of each experimental transition. For this subject, the first transition is from rest (R) to fast tilt (FT) and back, the second is from R to slow tilt (ST) and back, the third is from R to stand-up (SU) , then R to ST, R to SU and R to FT and back.. Transitions are randomized for each subject.

Figure 15: Instantaneous heartbeat statistics computed from an exemplary subject of the Tilt-Table protocol. In the top-left panel, the estimated $\mu_{RR}(t)$, superimposed on the recorded R-R series, and the instantaneous heartbeat standard deviation $\sigma_{RR}(t)$ are shown. Instantaneous sympathetic and parasympathetic activity, and sympatho-vagal balance as estimated through SAI and PAI, and SAI/PAI ratio measures, along with the LF, HF and LF/HF ratio are shown in the other panels. Vertical dotted red lines indicate the beginning and end of each experimental transition. For this subject, the first transition is from rest (R) to fast tilt (FT) and back, the second is from R to slow tilt (ST) and back, the third and fourth are from R to stand-up (SU) , then R to ST, and the final R to FT and back.. Transitions are randomized for each subject.